Physics – Uspekhi **50** (5) 529 – 553 (2007)

CONFERENCES AND SYMPOSIA PACS number: 01.10.Fv

Joint scientific session of the Physical Sciences Division of the Russian Academy of Sciences and Research Council of the P N Lebedev Physical Institute of the Russian Academy of Sciences honoring the 90th birthday of Academician V L Ginzburg (4 October 2006)

A joint scientific session of the Physical Sciences Division of the Russian Academy of Sciences (RAS) and Research Council of the P N Lebedev Physical Institute, RAS honoring the 90th birthday of Academician V L Ginzburg was held in the Conference Hall of the P N Lebedev Physical Institute, RAS on 4 October 2006. The following reports were presented at the session:

(1) **Gurevich A V** (P N Lebedev Physical Institute, RAS, Moscow) "Nonlinear effects in the ionosphere";

(2) **Kardashev N S** (P N Lebedev Physical Institute, RAS, Moscow) "The radio Universe";

(3) **Ptuskin V S** (Institute of Terrestrial Magnetism, Ionosphere and Radiowave Propagation, RAS, Troitsk, Moscow region) "On the origin of galactic cosmic rays";

(4) **Maksimov E G** (P N Lebedev Physical Institute, RAS, Moscow) "What is known and what is unknown about HTSCs";

(5) **Belyavsky V I, Kopaev Yu V** (P N Lebedev Physical Institute, RAS, Moscow) "Ginzburg – Landau equations for high-temperature superconductors";

(6) **Tsytovich V N** (A M Prokhorov Institute of General Physics, RAS, Moscow) "Polarization effects in a medium: from Vavilov – Cherenkov radiation and transition radiation to dust-particle pairing, or the development of one of V L Ginzburg's ideas from 1940 to 2006".

Extended reports Nos 1 and 4 in the form of reviews will be published in subsequent issues of *Physics – Uspekhi*. An abridge version of the other four papers is given below.

PACS numbers: **95.30.–k**, 95.55.Jz, 95.85.Bh
DOI: 10.1070/PU2007v050n05ABEH006214

The radio Universe

N S Kardashev

1. Introduction

In the 20th century, the revolutionary development of physics and technology made it possible to carry out studies of the Universe in all ranges of the electromagnetic spectrum. The discovery of cosmic radio emission from the Galaxy (K Jansky, 1932), from the Sun (G Reber, J Hey, J Southworth (1942 – 1944), and from galactic and extragalactic radio sources [G Reber, J Hey, S Parsons, J Phillips, J Bolton, G Stanley, M Ryle, F Smith (1942 – 1948)]; progress in radio astrospectroscopy and radio interferometry, and the discovery of quasars, pulsars, and cosmic microwave background in combination with deep analysis and modeling of observed astronomical objects on the basis of rapidly developing theoretical physics (quantum mechanics and General Relativity most of all) allowed building up the modern picture of the structure and evolution of individual astronomical objects and the multicomponent model of the entire Universe. In this rapidly developing scientific research, radio astronomical methods have played an outstanding role and will play it in years to come. Most references to the early period of radio astronomical studies can be found in the reference book [1], and the history of the development of radio astronomy in the USSR is described in Refs [2 – 6].

The first radio astronomical research in the USSR was initiated by Academician N D Papaleksi, the famous radio physicist, who was the head of the Laboratory of Oscillations at the Lebedev Physical Institute in the 1940s. When thinking over the possibility of the radio location of planets and the Sun, at the beginning of 1946 Papaleksi asked V L Ginzburg to investigate the reflection conditions of radio waves [7, p. 127]. For the Sun this turned out to be a difficult problem;

V L Ginzburg (left) and I S Shklovsky discuss problems in the theory of radio emission from solar corona (Rio de Janeiro, 1947).

Uspekhi Fizicheskikh Nauk **177** (5) 553 – 578 (2007)
Translated by K A Postnov, E N Ragozin, and M V Tsaplina;
edited by A Radzig and A M Semikhatov

Participants in the expedition to observe a solar eclipse in Brazil on May 20, 1947 on the deck of the motor ship *Griboedov*: S E Khaikin (far right, first row), Ginzburg and B M Chikhachev (fourth and ninth, respectively, second row), and I S Shklovsky (second from right, third row).

however, estimates and the analysis of peculiarities of the intrinsic emission of the Sun proved to be very interesting and initiated a series of pioneering papers on the physics of solar and galactic radio emission [7–20].

To observe the total eclipse of May 20, 1947, Papaleksi organized a big expedition to Brazil, in which Ginzburg and I S Shklovsky participated, in addition to experimentalists. A radio telescope (a re-equipped radar station with a receiver tuned to a wavelength of 1.5 m) was mounted on the deck of the motor ship *Griboedov*, and the ship itself turned following the Sun. The results of observations reliably showed for the first time that the meter-wavelength radio emission from the Sun is generated in the corona, in accordance with theoretical predictions. The discovery certificate was issued to Papaleksi, S E Khaikin, and B M Chikhachev. It was the first significant radio astronomical experiment in the USSR.

2. The most interesting results of recent years

The ultraprecise mapping of fluctuations of cosmic microwave background in the short-wavelength centimeter and millimeter ranges using the WMAP satellite (Wilkinson Microwave Anisotropy Probe) continues [21]. According to these data, the cosmological model is described by six dimensionless parameters:

$$\Omega_{\mathrm{m}} h^2 = 0.1277 + 0.0080/-0.0079\,,$$
$$\Omega_{\mathrm{b}} h^2 = 0.02229 \pm 0.00073\,,$$
$$h = 0.732 + 0.031/-0.032\,, \qquad n_{\mathrm{s}} = 0.958 \pm 0.016\,,$$
$$\tau = 0.089 \pm 0.030\,, \qquad \sigma_8 = 0.761 + 0.049/-0.048\,.$$

Here, Ω_{m} is the present matter density related to the critical density value, Ω_{b} is the same quantity for baryons, h is the modern value of the Hubble constant in the units of 100 km s^{-1} Mpc^{-1}, n_{s} is the power law index of the scalar density perturbations, τ is the optical depth, and σ_8 is the amplitude of density fluctuations on the scale of 8 Mpc. The combination of the WMAP data with observations from the Hubble Space Telescope suggests that the vacuum density in the Universe, $\Omega_{\Lambda} = 0.716 \pm 0.055$, puts constraints on the parameter of the dark energy equation of state, $w = -1.08 \pm 0.12$, and points to the very small deviation in the total matter density from the critical density: $\Omega_{\mathrm{c}} = -0.014 \pm 0.017$.

Even more precise data, including polarization measurements, are expected to be obtained by the Planck mission scheduled for launch in 2008 [22].

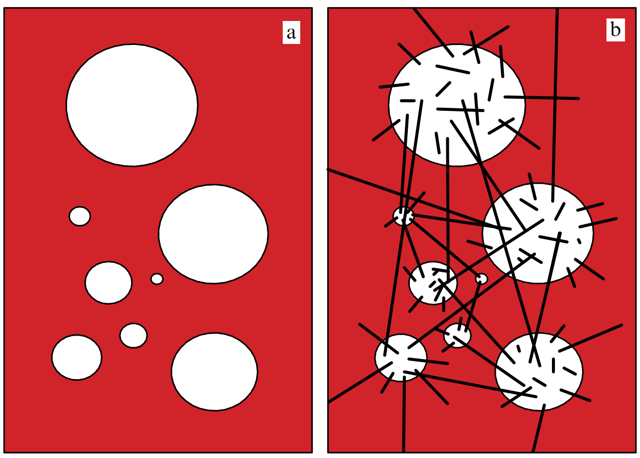

Figure 1. Models of the multielement Universe (Multiverse) without (a) and with (b) tunnels.

New prospects in cosmology are related to the model of the multicomponent Universe (the Multiverse), in which the inflationary stage occurs in different space regions at different instants of times (Fig. 1). Generally, the Multiverse can be infinite in space and time and infinitely diverse. Experimentally, such a model can be checked only if there are topological tunnels — wormholes [23, 24]. Paper [24] argues that wormholes can be supported by a strong magnetic field threading them (with a small portion of phantom energy), so observations of entrances to the tunnels can reveal some distinctive features like the monopole structure of a magnetic field, one-sided jets of relativistic particles, and the absence of an event horizon. However, for many indications such objects may have similarities with already observed galactic or extragalactic compact synchrotron sources.

Systematic studies of extragalactic sources [25] suggest that ultracompact objects which cannot be resolved with ground-based radio interferometers are observable in many galactic nuclei with supermassive black holes (or entrances to the tunnels) are located. The well-known radio galaxy M87 provides an example. Clearly, only with the use of space interferometers can the structure of such objects be studied and their nature understood.

A new (for radio astronomy) class of extragalactic sources emerging after gamma-ray bursts appears very intriguing. According to current models, these objects result from the explosion triggered in merging two stellar-mass black holes, or a black hole and a neutron star, or two neutron stars. Quite unexpectedly, the spectrum of these radio sources has been found to be inverted during the first days after the explosion [26, 27], i.e., it increases towards short wavelengths. This explains why the radiation flux from such sources barely changes with redshift and one can observe even the most distant explosions in the radio band [28]. Apparently, only with radio interferometers will we be able to study the structure of these objects and, in particular, to determine the directivity, dynamics and total energy of the explosion.

New discoveries in galactic radio astronomy are also very interesting. Observations of giant radio pulses from the Crab pulsar carried out at Pushchino and Kalyazin [29] (after special data processing to exclude pulse smearing due to the dispersion of radio waves propagating in the interstellar medium) revealed that some pulses have a giant amplitude with the flux exceeding that from the Sun and a brightness temperature of 10^{40} K. This means that the electromagnetic energy density in the pulse generation region exceeds that of the magnetic field of the neutron star itself, which is a big problem for the physical modeling of such regions.

In paper [30], the radio image of rapidly varying radio source Cygnus X-3 was obtained for the first time. This source represents a close binary system containing a black hole with a mass around five solar masses and a Wolf-Rayet star supplying matter to the accretion disk around the black hole. Studies of this system with high angular resolution will allow measurements of the structure and parameters of the plasma, relativistic particles, and magnetic field in the vicinity of black holes.

In 2006, a new class of pulsars was reported [31]: radio pulses with a period of 5.54 s were discovered from variable X-ray source XTE J1810-197. However, the radio emission spectrum turned out to be flat (in ordinary pulsars, the spectrum sharply decreases with frequency). This calls for a new model for coherent emission from these objects and allows studying them with record angular resolution at short wavelengths.

Of great interest are ongoing studies of ultracompact maser sources located in the Sstars and planetary systems formation regions. Observations of one of the most powerful maser sources in our Galaxy W3 (OH) at the wavelength of water vapor 1.35 cm [32] revealed the presence of a strong radio source which cannot be resolved by ground-based interferometers. Studies of star-forming galaxies show the presence of many narrow superpower lines (megamasers) at wavelengths of 1.35 cm (H_2O) and 18 cm (OH) generated in ultracompact regions (the upper limit to their size is inferred only from flux scintillations on inhomogeneities of the interstellar plasma) [33, 34].

3. Prospects of research

The prospects of radio astronomy are tightly connected to the most important problems of modern astrophysics and the possibility of building more powerful radio telescopes, first of all with better sensitivity and higher angular resolution. Here, it is very important to take into account many specific properties of the radio band. The main features and objectives of studies can be summarized as follows.

(1) The longest wavelengths of the electromagnetic spectrum ($\lambda = 0.1$ mm $-$ 10 km, eight orders of magnitude), the lowest frequencies, and the lowest energy quanta.

(2) The total intensity spectrum of cosmic electromagnetic background radiation reaching the absolute maximum in the radio band coinciding with the maximum of the cosmic microwave background spectrum which lies entirely in the radio band.

(3) The spectrum of spatial fluctuations of the intensity and polarization of the cosmic microwave background tightly related to the parameters of the early Universe, dark matter, and dark energy.

(4) The lowest-temperature objects (from 300 K down to 2.73 K and even to -2.73 K, with gradients as low as 10^{-6} K) studied in the radio band.

(5) Objects with the uppermost brightness temperature (up to 10^{40} K), which is due to the possibility of coherent emission, studied in the radio band.

(6) The scattering of cosmic microwave background radiation from electrons (the Zel'dovich – Sunyaev effect on galaxy clusters) studied in the radio band.

(7) The possibility of studying the interstellar matter of our Galaxy and other galaxies (structure, dynamics, and evolution) probed by the 21-cm line of neutral hydrogen (hyperfine splitting of the ground level), and by lines of other elements and molecules.

(8) Emission from interstellar dust (with observed temperatures down to 7 K and below) studied in the radio band. Dust clouds are transparent for radio waves (the wavelength exceeds the size of the dust grains), hence the possibility of studying the planetary formation processes.

(9) Radio emission of ionized plasma in the continuum and recombination lines (transitions between the uppermost atomic energy levels) in galaxies, the possibility of observing recombination of the Universe, the dark age, the primeval star formation.

(10) The dispersion effect of radio waves propagating in a plasma (measurements of the dispersion measure, DM).

(11) Scintillation of radio sources (turbulence of interplanetary and interstellar plasma).

(12) Measurement of Faraday rotation and Zeeman splitting.

(13) Synchrotron radio radiation from relativistic electrons and the possibility of discovering synchrotron radio emission of relativistic protons (sources of cosmic rays).

(14) Studies of cosmic rays and ultrahigh energy neutrinos: the coherent radio emission generated by high-energy particles impacting a solid body (for example, the Moon) — the Askaryan effect.

(15) Studies of radio emission from supernova shells as possible cosmic ray acceleration sites.

(16) Ultrahigh angular resolution studies into the structure of the vicinity of black holes as possible sites of relativistic particle acceleration (the source Sgr A* in the galactic center, nuclei of other galaxies, radio galaxies, quasars, microquasars, 'superluminous' motion and expansion).

(17) Ultrahigh resolution searches for topological tunnels (wormholes), testing string theory and theories with extra dimensions, studies of observational appearances of the Multiverse.

(18) Radio emission at the plasma frequency and gyrofrequencies: Sun and radio stars.

(19) Studies of the most compact radio sources — pulsars (neutron and quark stars, magnetars, giant pulses), binary pulsars, gravitational wave emission by pulsars.

(20) Masers (brightness temperatures up to 10^{16} K), megamasers, antimasers.

(21) In the radio band, record angular resolution being achieved — up to several dozen microarcseconds (interferometers, multielement arrays, aperture synthesis, multifrequency synthesis). There are prospects for space radio interferometry with angular resolution up to several microarcseconds and even nanoarcseconds, three-dimensional astronomy, interstellar interferometer, the Universe in the near zone.

(22) The most precise coordinate accuracy, proper motions, and parallaxes.

(23) Record brightness-temperature sensitivity (receivers and bolometers taking into the account boundary between quantum and classical statistics, near the maximum of the relic background, being close to realization).

(24) The most accurate timing (nanoseconds, the pulsar time scale).

(25) Low radio wave attenuation allowing studies of the surfaces of planets through cloud layers (Venus) and even subsurface layers (the Moon, with prospects for Mars, etc.).

(26) Coherent radio emission from particles in the magnetosphere of Earth, Jupiter, and, possibly, other planets with strong magnetic fields.

(27) The radio band being optimal for communication with possible extraterrestrial civilizations.

(28) Possibility of building telescopes in the radio band, which observe simultaneously almost the whole sky, and it is very important for studying short-duration phenomena.

(29) In radio astronomy there is the possibility of building telescopes with the largest collecting areas (expenses are inversely proportional to the wavelength).

(30) In space there is no technical or atmospheric radio interference (in the submillimeter and millimeter bands, nor for bands below the critical ionospheric frequency). This opens new prospects for the construction of radioastronomical observatories. The absence of the force of gravity is favorable too (only tidal forces remain).

Basic parameters of the RadioAstron mission

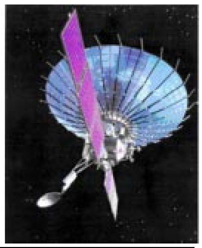

Range (λ, cm)	92	18	6.2	1.2 – 1.7
Band width ($\Delta\nu$, MHz)	4	32	32	32
Interference beam width (microarcsec) for the base of 350,000 km	540	106	37	7.1 – 10
Flux sensitivity (σ, mJy), ground based antenna EVLA, 300 s exposition	10	1.3	1.4	3.2

Figure 2. Basic parameters of the Earth – space interferometer (the RadioAstron project).

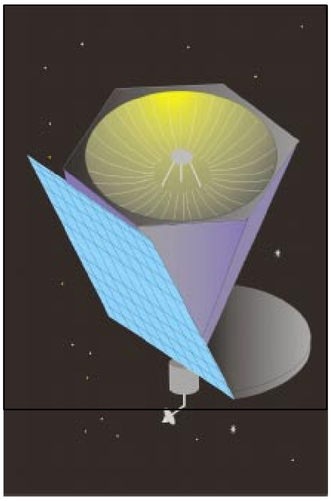

Antenna diameter 12 m
Spectral range 0.01 – 20 mm

Bolometric sensitivity (wavelength 0.3 mm, 1 h exposition) of 5×10^{-9} Jy (σ)

Sensitivity of the Earth – space interferometer (ALMA) (wavelength 0.5 mm, bandwidth 16 GHz, 300 s exposition) of 10^{-4} Jy (σ)
Interference beam width up to 10^{-9} arcseconds

Figure 3. Basic parameters of the Millimetron project.

The largest radio astronomical space projects providing ultrahigh angular resolution include Earth-space interferometers RadioAstron, designed for observations at centimeter and decimeter wavelengths (basic parameters are shown in Fig. 2 and described in more detail in Ref. [35]), and Millimetron designed for observations in the millimeter and submillimeter ranges (basic parameters are shown in Figs 3 and 4, see Ref. [36] for more detail). The ground-based segment in both cases will include all the world's largest radio telescopes. Both projects are included in the Russian Federal Space Program and are supported by broad international cooperation of research institutes and observatories. New ground-based radio telescopes are under construction. In particular, the Russian Federation, in cooperation with Uzbekistan, is building at the Suffa Plateau the largest millimeter-wavelength radio telescope with a mirror diameter of 70 m [37], the international ALMA (Atakama Large Millimeter Array) consisting of 64 12-m antennas is under construction at an altitude of 5 km in the Atakama desert [38]. The building of the largest multibeam radio (meter and decameter) telescope in Europe, LOFAR (Low Frequency Array), with an effective area of up to million square kilometers [39] has started, as well as the design of the

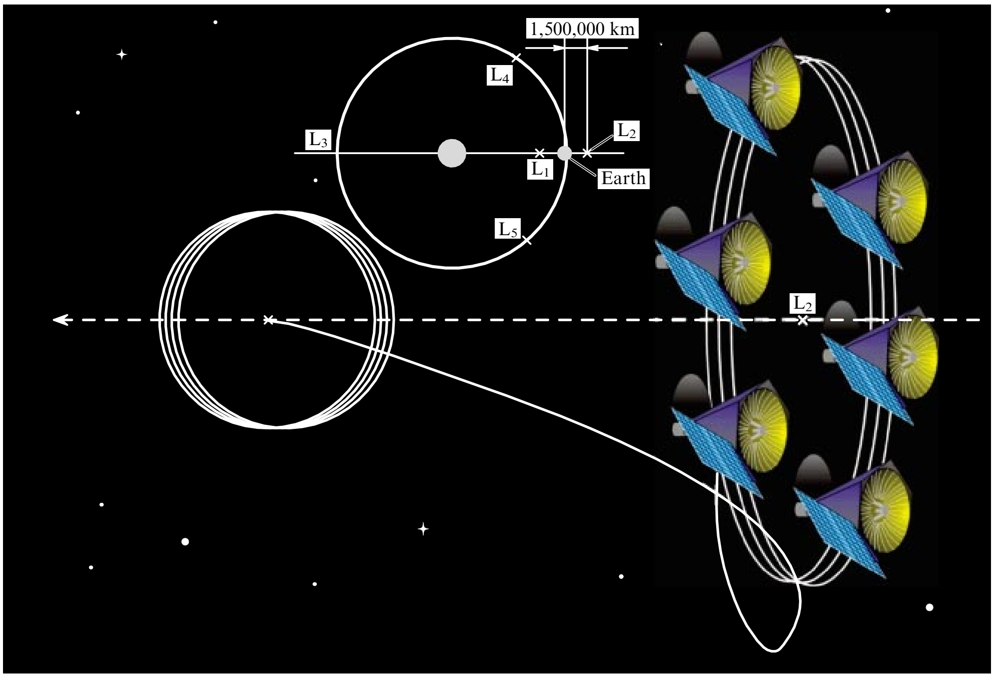

Figure 4. Space multielement interferometer.

centimeter- and decimeter-wavelength SKA (Square Kilometer Array) radio telescope of an equal area [40]. Under preliminary discussion is the construction of new multielement antenna arrays in space [similar to the scheme of the possible development of the Millimetron project (see Fig. 4)]: in the vicinity of the antisolar Lagrangian point L_2 (1.5×10^6 km from Earth) or even near the 'triangular' points (150×10^6 km). In that case, the entire Universe will fall into the near Fresnel zone for the submillimeter range.

4. Conclusions

The basic problems of astrophysics from the point of view of science at the beginning of the 21st century mainly coincide with the list of astrophysical problems discussed in the book [7, pp. 11 – 74], but I would like to emphasize the importance of reductionism to understand the role of the processes of the origin and evolution of life and information in the Universe.

(1) The highest forms of intelligence in the Universe. The problem of reductionism.

(2) The anthropic principle and the Multiverse.

(3) Topology of the Universe, extra dimensions, wormholes.

(4) The cosmological model and evolution of our Universe.

(5) Dark matter and dark energy.

(6) The beginning of our Universe.

(7) Galactic nuclei and black holes.

(8) Neutron stars, quark and preon stars, origin of cosmic gamma-ray bursts.

(9) Planetary systems and condensed matter in the Universe, origin and evolution of life.

(10) Gravitational wave astrophysics and relic gravitational waves.

(11) Neutrino astrophysics and relic neutrinos.

(12) Origin of cosmic rays.

Radio astronomy has brilliant prospects for solving these issues based on the theory of propagation and generation of radio waves in cosmic media, the physics of cosmic rays and other fields of physics and astrophysics, many of which were elaborated by V L Ginzburg. In conclusion, I would like to deeply thank him for discussions of the problems mentioned here.

References

1. Neishil'd V G, Panovkin B N (Compilers); Kokurin Yu L (Executive Ed.) *Radioastronomiya* Annotir. Bibliogr. Ukazatel' Otechestv. i Inostr. Literatury. 1932 – 1958 gg. (Radio Astronomy. Annotated Reference Guide to Russian and Foreign Papers. 1932 – 1958) (Moscow: Izd. AN SSSR, 1960)
2. Salomonovich A E et al. (Editorial Board) *Ocherki Istorii Radioastronomii v SSSR* Sb. Nauch. Tr. (Essay on the History of Radio Astronomy in the USSR. Coll. of Papers) (Kiev: Naukova Dumka, 1985); Gindilis L M et al. *Razvitie Radioastronomii v SSSR* (Development of Radioastronomy in the USSR) (Executive Ed. A E Salomonovich) (Moscow: Nauka, 1988)
3. Alekseev V A et al. *Sovetskie Radioteleskopy i Radioastronomiya Solntsa* (Soviet Radio Telescopes and Radio Studies of the Sun) (Executive Eds A E Salomonovich, G Ya Smol'kov) (Moscow: Nauka, 1990)
4. Shklovskii I S *Iz Istorii Razvitiya Radioastronomii v SSSR* (Novoe v Zhizni, Nauke, Tekhnike: Kosmonavtika, Astronomiya, Vyp. 11) [From the History of Radio Astronomy in the USSR (New in Life, Science, Techniques: Cosmonautics, Astronomy, Issue 11)] (Moscow: Znanie, 1982)
5. Ginzburg V L (Executive Ed.) *Radioastronomiya. Trudy Pyatogo Soveshchaniya po Voprosam Kosmogonii, 9 – 12 Marta 1955 g.* (Radio Astronomy. Proc. of the Fifth Meeting on Problems in Cosmogony, 9 – 12 March 1955) (Moscow: Izd. AN SSSR, 1956)
6. Van de Hulst H C (Ed.) *Radio Astronomy, IAU Symp., No. 4, August 1955* (Cambridge: Univ. Press, 1957)
7. Ginzburg V L *O Nauke, o Sebe i o Drugikh* (About Science, Myself, and Others) 3rd ed. (Moscow: Fizmatlit, 2003) [Translated into English (Bristol: IOP Publ., 2005)]
8. Ginzburg V L "Ob izluchenii Solntsa v oblasti radiochastot" ("On the radio emission from the Sun") *Dokl. Akad. Nauk SSSR* **52** 491 (1946)
9. Ginzburg V L "Radioizluchenie Solntsa i Galaktiki" ("Radio emission from the Sun and the Galaxy") *Usp. Fiz. Nauk* **32** 26 (1947)

10. Ginzburg V L "Novye dannye o radioizluchenii Solntsa i Galaktiki" ("New data on radio emission from the Sun and the Galaxy") *Usp. Fiz. Nauk* **34** 13 (1948)
11. Ginzburg V L "N.D. Papaleksi i radioastronomiya" ("N.D. Papaleksi and radio astronomy") *Izv. Akad. Nauk SSSR Ser. Fiz.* **12** 34 (1948)
12. Ginzburg V L "O pogloshchenii radiovoln v solnechnoi korone" ("On the absorption of radio waves in solar corona") *Astron. Zh.* **26** 84 (1949)
13. Getmantsev G G, Ginzburg V L "O difraktsii solnechnogo i kosmicheskogo radioizlucheniya na Lune" ("On the diffraction of solar and cosmic radio emission on the Moon") *Zh. Eksp. Teor. Fiz.* **20** 347 (1950)
14. Ginzburg V L "Kosmicheskie luchi kak istochnik galakticheskogo radioizlucheniya" ("Cosmic rays as the source of galactic radio emission") *Dokl. Akad. Nauk SSSR* **76** 377 (1951)
15. Ginzburg V L "Mezhzvezdnaya materiya i ionosfernye vozmushcheniya, privodyashchie k mertsaniyu radiozvezd" ("Interstellar matter and ionospherical perturbations leading to scintillation of radio stars") *Dokl. Akad. Nauk SSSR* **84** 245 (1952)
16. Ginzburg V L "Sverkhnovye i novye zvezdy kak istochniki kosmicheskogo i radioizlucheniya" ("Supernovae and novae stars as sources of cosmic radio emission") *Dokl. Akad. Nauk SSSR* **92** 1133 (1953)
17. Al'pert Ya L, Ginzburg V L, Feinberg E L *Rasprostranenie Radiovoln* (Propagation of Radio Waves) (Moscow: Gos. Izd. Tekhn.-Teor. Lit., 1953)
18. Ginzburg V L "O prirode radiogalaktik" *Astron. Zh.* **38** 380 (1961) ["On the nature of the radio galaxies" *Sov. Astron.* **5** 282 (1961)]
19. Ginzburg V L, Pisareva V V "Polyarizatsiya radioizlucheniya diskretnykh istochnikov i izuchenie metagalakticheskogo, galakticheskogo i okolosolnechnogo prostranstva" ("Polarization of radio emission of discrete sources and the study of metagalactic, galactic, and near-solar space") *Izv. Vyssh. Uchebn. Zaved. Radiofiz.* **6** 877 (1963)
20. Ginzburg V L, Syrovatskii S I *Proiskhozhdenie Kosmicheskikh Luchei* (The Origin of Cosmic Rays) (Moscow: Izd. AN SSSR, 1963) [Translated into English (Oxford: Pergamon Press, 1964)]
21. Spergel D N et al. "Wilkinson microwave anisotropy probe (WMAP) three year results: implications for cosmology", astro-ph/0603449; *Astrophys. J.* (2007) (in press)
22. The Planck Collab. "The scientific programme of Planck", astro-ph/0604069
23. Visser M *Lorentzian Wormholes: from Einstein to Hawking* (Woodbury, NY: American Institute of Physics, 1995)
24. Kardashev N S, Novikov I D, Shatskii A A "Magnitnye tonneli (krotovye nory) v astrofizike" *Astron. Zh.* **83** 675 (2006) ["Magnetic tunnels (wormholes) in astrophysics" *Astron. Rep.* **50** 601 (2006)]
25. Kovalev Y Y et al. "Sub-milliarcsecond imaging of quasars and active galactic nuclei. IV. Fine-scale structure" *Astron. J.* **130** 2473 (2005)
26. Kuno N et al. "Radio observations of the afterglow of GRB 030329" *Publ. Astron. Soc. Jpn.* **56** (2) L1 (2004); astro-ph/0401258
27. Kohno K et al. "Nobeyama Millimeter Array observations of GRB 030329: a decay of afterglow with bumps and molecular gas in the host galaxy" *Publ. Astron. Soc. Jpn.* **57** (1) 147 (2005); astro-ph/0412261
28. Frail D A et al. "An energetic afterglow from a distant stellar explosion" *Astrophys. J.* **646** L99 (2006)
29. Soglasnov V A et al. "Giant pulses from PSR B1937+21 with widths $\leqslant 15$ nanoseconds and $T_b \geqslant 5 \times 10^{39}$ K, the highest brightness temperature observed in the Universe" *Astrophys. J.* **616** 439 (2004)
30. Tudose V et al. "First e-VLBI observations of Cygnus X-3" *Mon. Not. R. Astron. Soc. Lett.* **375** L11 (2007)
31. Camilo F et al. "Transient pulsed radio emission from a magnetar" *Nature* **442** 892 (2006)
32. Slysh V I "Self-stark limit on brightness temperature in cosmic masers", in *Radio Astronomy at the Fringe* (Astron. Soc. of the Pacific Conf. Ser., Vol. 300, Eds J A Zensus, M H Cohen, E Ros) (San Francisco, Calif.: Astron. Soc. of the Pacific, 2003) p. 239
33. Vlemmings W H T, Bignall H E, Diamond P J "Green Bank Telescope observations of the water masers of NGC 3079: accretion disk magnetic field and maser scintillation" *Astrophys. J.* **656** 198 (2007)
34. Argon A L et al. "Toward a new geometric distance to the active galaxy NGC4258: I. VLBI monitoring of water maser emission", astro-ph/0701396
35. RadioAstron Mission, http://www.asc.rssi.ru/radioastron/description/intro_eng.htm
36. Millimetron Project, http://www.asc.rssi.ru/millimetron/eng/millim_eng.htm
37. Radioastronomicheskaya observatoriya na plato Suffa (Radio astronomical observatory on the Suffa plateau), http://tashkbm.narod.ru/suffa.htm
38. The Atakama Large Millimeter/submillimeter Array (ALMA), http://www.alma.info/
39. LOFAR, http://www.lofar.org/
40. Square Kilometre Array (SKA), http://www.skatelescope.org/

PACS numbers: 96.50.S –, 98.70.Sa
DOI: 10.1070/PU2007v050n05ABEH006216

On the origin of galactic cosmic rays

V S Ptuskin

1. Introduction

Our Galaxy is filled with cosmic rays — that is, a gas consisting of relativistic protons, electrons, and atomic nuclei. Most of these particles were accelerated in supernova remnants and wander in the interstellar magnetic fields over several dozen million years before exiting into intergalactic space. The energy spectrum of cosmic rays has a power-law form with a break (a knee) at 3×10^{15} eV (Fig. 1). The maximum detected energy exceeds 10^{20} eV. With a tiny number density of particles, $N \sim 10^{-10}$ cm^{-3}, which is 10 orders of magnitude smaller than the average interstellar gas density in the galactic disk, $n \sim 1$ cm^{-3}, cosmic rays have the energy density $w_{\mathrm{cr}} = 1.5$ eV cm^{-3}, which is comparable to the energy density of galactic magnetic fields and the energy density of turbulent interstellar gas motions. Cosmic

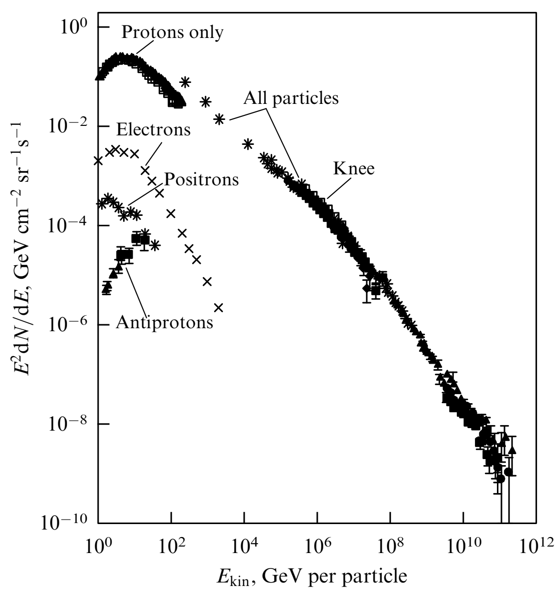

Figure 1. Cosmic ray spectrum with energies exceeding 1 GeV. (Simplified version of the figure from paper [1], where references to the corresponding experiments can be found.)

rays are highly isotropic — the amplitude of the first harmonic of their angular incoming direction distribution is $\delta_{\rm cr} \sim 10^{-3}$ at energies $10^{12}-10^{14}$ eV, where the data are the most robust.

The effective isotropization and mixing of trajectories of charged energetic particles are explained by the action of interstellar magnetic fields. As a result, the direct identification of sources of particles reaching the Earth proves to be impossible. Establishing the synchrotron nature of the main part of nonthermal space radio emission at the beginning of the 1950s enabled probing the properties of remote relativistic electrons of cosmic rays. It is during this period the pioneering papers by V L Ginzburg [2–4] on the theory of cosmic synchrotron radio radiation appeared. Progress in radio astronomy led to the appearance of the astrophysics of cosmic rays and made it clear that the presence of relativistic particles is a universal phenomenon in space conditions. The initial period of development of cosmic ray astrophysics is described in more detail in paper [5] and references cited therein. To the mid-1960s, mostly due to studies conducted by Ginzburg and his collaboration with S I Syrovatskii, the canonical model for the origin of cosmic rays was elaborated (see the monograph by Ginzburg and Syrovatskii [6]). This book became the bible for high-energy astrophysicists. The model developed in Ref. [6] is based on the following statements: most cosmic rays have a galactic origin; cosmic rays diffuse in interstellar magnetic fields and fill up an extended halo, and supernova explosions are the sources of cosmic rays. The booming development of this field of astrophysics is reflected in the book [7], which was intended by Ginzburg as a continuation of the monograph [6]. Book [7] includes, in particular, new topics: gamma-ray astronomy, neutrino astronomy, ultrahigh energy cosmic rays, and the description of acceleration and propagation of cosmic rays on the kinetic level. Later reviews can be found in Refs [8–10]. The present short communication mainly illustrates the developments of studies carried out by Ginzburg and his scientific school. Basically, the results obtained after issuing the review [8] in *Physics–Uspekhi* are mainly included and unsolved problems are formulated.

2. Diffusion model of cosmic ray propagation

The motion of cosmic rays with energies below $E \sim 10^{17}$ eV in galactic magnetic fields is usually described as diffusion [6, 7]. The diffusion model constitutes the base for interpreting the spectrum, composition, and anisotropy of cosmic rays, as well as the corresponding radio, X-ray, and gamma-ray astronomical observations. The consistency of these data allows the determination of the basic model parameters. To this end, it is necessary to solve the transport equation for relativistic protons, nuclei, and electrons for a given distribution of sources (supernova remnants) and halo boundary conditions. The transport equation for particles describes their diffusion, convective transfer by the hypothetical galactic wind, and energy changes due to energy losses in the interstellar medium, as well as possible additional acceleration by interstellar turbulence. Cosmic rays also contain secondary nuclei like ^{2}H, ^{3}He, Li, Be, B and some others that are rarely observed in nature, which are produced by the spallation of heavier nuclei interacting with nuclei of the interstellar gas. Over the time spent in the Galaxy, cosmic rays traverse a matter thickness of ~ 10 g cm^{-2} at an energy of ~ 1 GeV per nucleon (at this energy, the maximum ratio of primary to secondary nuclei is observed). Modern detailed calculations of the propagation and nuclear transformation of cosmic rays in the Galaxy include around hundred different stable and radioactive isotopes in the broad energy range.

To model cosmic ray propagation, both the combination of analytical and numerical methods (see Refs [11–14]) and direct numerical calculations [15, 16] are employed. The required total power of cosmic ray sources in the Galaxy is estimated to be $Q_{\rm cr} = 5 \times 10^{40}$ erg s^{-1}, which corresponds to about 15% of the kinetic energy of supernova explosions. Accounting for the selection of ions injected into the acceleration process by the value of the first ionization potential or volatility, the elemental composition of cosmic rays in the sources turns out to be close to that of the solar system and local interstellar medium (see Ref. [9] for more detail). The height of the cosmic ray halo is $H \approx 4$ kpc (or more in the model with galactic wind). According to Ref. [16], the diffusion coefficient of cosmic rays in two main versions of the diffusion model as obtained from statistically reliable data (up to about 100 GeV per nucleon) on secondary nuclei is expressed in the form

$$D = 2.2 \times 10^{28} \beta \left(\frac{R}{R_0}\right)^{0.6} [\mathrm{cm^2\ s^{-1}}] \quad \text{for} \quad R > R_0 = 3\ \mathrm{GV}\,,$$
$$D \sim \beta^{-2} \quad \text{for} \quad R < R_0 \tag{1}$$

in the pure diffusion model, and

$$D = 5.2 \times 10^{28} \beta \left(\frac{R}{R_0}\right)^{0.34} [\mathrm{cm^2\ s^{-1}}] \quad \text{at all } R \tag{2}$$

taking into account additional stochastic acceleration of particles by random magnetohydrodynamic (MHD) waves in the interstellar medium with the Alfvén velocity $V_{\rm a} \approx 36$ km s^{-1} (see also the discussion in Section 3). Here, $R = pc/Z$ is the magnetic rigidity, p is the momentum, Z is the charge, $\beta = v/c$, and v is the particle velocity.

Neither variant (1) nor (2) is problem-free and both require improvement. The strong energy dependence of the diffusion in Eqn (1) in the pure diffusion model leads to an anisotropy exceeding what is observed by more than an order of magnitude at energies $\sim 10^{14}$ eV (see Ref. [17]). On the other hand, the model with additional acceleration gives values of the secondary antiproton flux in cosmic rays lower than those observed (see Ref. [16]). It is also essential that in order to explain the energy spectrum of cosmic rays $\sim E^{-2.7}$, observed for energies $E > 30$ GeV per nucleon, the spectrum in the source be $E^{-2.1}$ in variant (1), and $E^{-2.36}$ in variant (2). Direct measurements of radio and gamma-ray emissions from supernova remnants and the modern theory of particle acceleration in supernova remnants suggest a particle spectrum close to E^{-2}, and in this sense variant (1) looks more attractive.

Diffuse gamma-ray emission reflects the global distribution of cosmic rays in the Galaxy. When interacting with interstellar gas nuclei, the proton-nuclear component of cosmic rays generates continuous gamma-ray emission mainly via the creation and decay of π^0-mesons in the process $\mathrm{pp} \to \pi^0 \to \gamma\gamma$. The electron component generates gamma-ray emission by the Compton scattering of interstellar background photons and via bremsstrahlung emission in the interstellar gas. The diffusion model of cosmic ray propagation with the diffusion coefficient which is inferred from near-

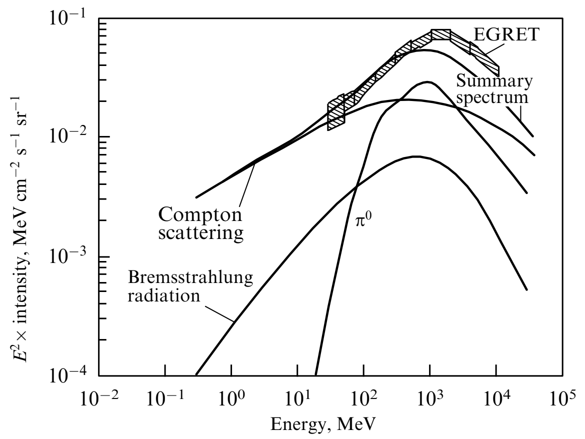

Figure 2. Spectrum of the diffuse galactic gamma-ray emission [19]: the EGRET observational data and results of the corresponding theoretical calculations for different generation mechanisms of gamma-ray emission.

Earth observations and is independent of coordinates everywhere in the Galaxy generally well reproduces the angular and energy distribution of galactic gamma-rays with energies 30 MeV – 10 GeV, obtained by the EGRET (Energetic Gamma Ray Experiment Telescope) experiment [18, 19]. However, the gradient of cosmic ray density was found to be smaller than the predicted one assuming the standard radial distribution of the sources of supernova remnants, which, most likely, calls for improvement of the model (see Ref. [20]).

An enigmatic feature of the EGRET data is an isotropic excess of gamma-ray emission at energies of 1 – 10 GeV with respect to the expected flux calculated using spectral data on protons, nuclei, and electrons observed in cosmic rays near the Earth (Fig. 2). Unless this is an instrumental effect [which will be tested by the GLAST (Gamma-ray Large Area Space Telescope) mission scheduled for launch shortly], the presence of an anomaly in the cosmic ray characteristics in the neighborhood of the solar system is not excluded on a scale of about several hundred parsecs compared to the mean galactic values. There are alternative explanations related to the contribution of hard-spectrum sources to the diffuse emission [21, 22] and to the gamma-ray flux from the hypothetical dark matter annihilation in the galaxy with an extended halo [23]. Here, observations of diffuse gamma-ray emission from the galactic disk at energies of several TeV [24] seem to be very instructive (see the discussion in Ref. [25]).

Note that according to the EGRET data, the application of the 'Ginzburg test' allowed establishing [26] that the number density of cosmic rays with the energies of 1 – 10 GeV in intergalactic space is significantly less than in the Galaxy. The test proposed in Ref. [27] suggests measuring the gamma-ray flux from the Magellanic Clouds in which the mass of gas and the distance are well known. As an elaboration of another earlier paper [28], in which Ginzburg participated, a strong limit on the intergalactic cosmic ray density on cosmological scales was recently obtained [29]. It was shown that cosmic rays accelerated in supernovae and starburst galaxies have an appreciable effect on the thermal history of the Universe at high redshifts. To explain the intergalactic medium temperature of $\sim 10^4$ K at redshifts $z = 2-4$, the present-day energy density (i.e., at $z = 0$) of cosmic rays in intergalactic space must be $10^{-4} - 6 \times 10^{-3}$ eV cm^{-3} under different assumptions in the standard cold dark matter cosmological model with the Λ-term. This value is consistent with the known energy estimates [6 – 8].

3. Kinetic theory of diffusion

The diffusion of cosmic rays in the Galaxy is explained by their scattering in random magnetic fields. This scattering has a resonance character, so that a particle with gyroradius $r_g = pc/(ZeB)$ is mainly scattered off magnetic field inhomogeneities with the wave number $k_{res} \sim 1/r_g$ (see Refs [7, 30]). In the typical interstellar field $B = 5$ μG, the gyroradius is $r_g = 6.7 \times 10^{11} R_{GV}$ [cm] (here, R_{GV} is the magnetic rigidity of a particle measured in gigavolts). The emerging spatial diffusion turns out to be strongly anisotropic and preferentially occurs along the magnetic field lines. However, strong fluctuations $\delta B/B \sim 1$ on large scales $L \sim 100$ pc make the diffusion isotropic [in a quasistatic field, the diffusion isotropization is nontrivial and is due to stochastic divergence of close magnetic field lines (see Refs [31, 32])]. Assuming magnetic field fluctuations on the resonance scale to be small compared to the total large-scale field, $\delta B_{res} \ll B$, and fluctuations to be isotropic in the space of wave vectors $\mathbf{k}$, one can estimate the diffusion coefficient for $r_g < L$ (i.e., for $E < 10^{17} Z$ [eV]) as the following:

$$D \approx \frac{v r_g}{3} \frac{B^2}{B_{res}^2} \tag{3}$$

(see Refs [7, 30] for more detail). The observed spectral energy density of the interstellar turbulence has a power-law form: $w(k)\,dk \sim k^{-2+a}\,dk$, where $a \approx 1/3$ in the broad range of wave numbers, $1/(3 \times 10^{20}) < k < 1/10^8$ cm^{-1} [33]. Then, formula (3) yields the estimate $D \approx 4 \times 10^{27} R_{GV}^{1/3}$ [cm^2 s^{-1}], which is consistent with the empirical value in the model with additional acceleration (2). The additional acceleration itself appears as momentum diffusion with the coefficient $D_{pp} \approx p^2 V_a^2/D$ taking into account a finite velocity of motion ($\sim V_a$) of random inhomogeneities which scatter off particles and provide spatial diffusion. The additional acceleration by the interstellar turbulence can be significant only at relatively small energies and does not affect the energy spectrum of cosmic rays for $E > 30$ GeV per nucleon. Recall that the main acceleration occurs in compact sources — supernova remnants.

The dependence of the diffusion on the magnetic rigidity of particles, $D \sim \beta R^{1/3}$, is typical for the Kolmogorov spectrum for which $a = 1/3$. Theoretically [34], it cannot be excluded that the Kolmogorov spectrum relates only to some part of the interstellar MHD turbulence which includes Alfvén type perturbations strongly elongated along the magnetic field direction. Such perturbations with $\mathbf{kB} = 0$ are ineffective for particle scattering and cannot reproduce the required diffusion coefficient. At the same time, more isotropic perturbations consisting of fast magnetosonic waves with smaller amplitude on the principal scale can exist [35]. This part of turbulence has the Iroshnikov – Kraichnan-like spectrum with parameter $a = 1/2$ and provides the diffusion of cosmic rays with diffusion coefficient $D \sim \beta R^{1/2}$, which is close to the empirical model value (1) if $\delta B/B \sim 0.2$ for these perturbations on the principal scale $L \sim 100$ pc. Notice that here one can explain why the diffusion coefficient (1) has a minimum at $R = R_0 = 3$ GV: a comparatively slow nonlinear Iroshnikov – Kraichnan cascade of the MHD waves cuts off on scales smaller than $1/k \sim 10^{12}$ cm due to damping on cosmic rays. The corresponding self-consistent calculations were done in Ref. [16].

One can state that the kinetic theory gives the diffusion coefficient consistent with the empirical value and in principle explains its dependence on the magnetic rigidity. However, the absence of detailed information on interstellar turbulence makes it impossible to obtain unique predictions and, in particular, to make the ultimate choice between the variants $D \sim \beta R^{1/3}$ and $D \sim \beta R^{1/2}$.

The presence of a nonzero large-scale mean magnetic field in the Galaxy leads to the appearance of the Hall diffusion with the coefficient $D_{\rm H} = vr_{\rm g}/3$ which emerges in the antisymmetric part of the diffusion tensor and is strongly dependent on the magnetic rigidity of particles. Owing to this last circumstance, the role of the Hall diffusion (drift) increases with energy, which can lead to the appearance of the knee in the cosmic ray spectrum at energies $\sim 3 \times 10^{15}$ eV due to the passage from the ordinary diffusion to the Hall one [36–38]. Another explanation relates the origin of the bend to particle acceleration processes in supernova remnants (see Section 6).

4. Collective effects in cosmic rays

Cosmic rays cannot always be considered to be free test particles moving in given regular and random fields. Ginzburg wrote the pioneering paper on the role of collective (plasma) effects during cosmic ray propagation [39] (see also Ref. [40]). The stream instability of cosmic rays with the particle density $N_{\rm cr}(E) \sim E^{-\gamma+1}$ amplifies MHD waves with the growth rate

$$\Gamma_{\rm cr}(k) \approx \Omega_{\rm p}\,\frac{N(r_{\rm g} > k^{-1})}{n}\left(\frac{v\delta_{\rm cr}}{(\gamma+2)V_{\rm a}} - 1\right), \qquad (4)$$

where $\Omega_{\rm p}$ is the gyrofrequency of thermal protons. Even for a small anisotropy $\delta_{\rm cr} \approx 10^{-3}$, the instability for galactic cosmic rays with energies ~ 100 GeV develops in about 10^5 years, i.e., rather rapidly for the galactic timescale. The development of the instability leads to isotropization of the angular distribution of particles and turbulence enhancement (see, for example, the papers [41–43] and references cited therein). The effect is more significant close to the sources. As we shall see from the discussion in Section 6, the development of the stream instability of particles at the shock front in a supernova remnant is a prerequisite for cosmic ray acceleration.

Cosmic rays induce, in addition to kinetic effects, significant hydrodynamic effects in the Galaxy. Accounting for cosmic ray pressure is principally important for the formation of a halo filled with gas, a magnetic field, and relativistic particles [44]. The equilibrium distribution of the interstellar medium above the galactic plane in the gravitational field of stars is subjected to the Parker instability [45]. Cosmic rays play a significant role in the development of this instability. Using the diffusion–convective transport equation for cosmic rays, one can show [46] that the instability develops if the polytropic index of the interstellar gas $\gamma_{\rm g}$ turns out to be less than the critical value

$$\gamma_{\rm g^*} = 1 + \frac{P_{\rm m0}}{P_{\rm g}}\,\frac{0.5P_{\rm g} + P_{\rm m0} + P_{\rm cr}}{P_{\rm g} + 1.5P_{\rm m0} + P_{\rm mt} + P_{\rm cr}}\,, \qquad (5)$$

where $P_{\rm g}$, $P_{\rm m0}$, $P_{\rm mt}$, and $P_{\rm cr}$ are the pressures of gas, regular and random galactic magnetic fields, and cosmic rays, respectively. The instability gives rise to large-scale turbulence and helps sustain an almost equipartition energy distribution among cosmic rays, magnetic fields, and turbulent gas motions. The characteristic time for instability development is $\sim 10^7$ years in the gaseous disk of the Galaxy, and $\sim 10^8$ years in the gas halo. Paper [47] showed that magnetic arches and loops appearing above the galactic disk due to the action of cosmic rays are necessary for a $\alpha\omega$-dynamo to operate, which is the primary mechanism of magnetic field generation in the Galaxy.

It is possible that the gas in the halo is not in static equilibrium but is involved in large-scale convective motions (the galactic wind). The existence of the supersonic galactic wind in our Galaxy due to the high temperature of the interstellar gas in the galactic disk appears unlikely since the actual gas temperature is not high enough. However, the galactic wind can be supported by cosmic ray pressure. In Refs [48, 49], a model is constructed in which cosmic rays, after leaving the sources (supernova remnants), determine the wind outflow in the rotating Galaxy with a frozen magnetic field. Here, the stream instability of cosmic rays exiting the Galaxy along the spiral magnetic field leads to the MHD turbulence generation, which self-consistently determines the transfer of relativistic particles. The outflow velocity is ~ 30 km s^{-1} at a distance of ~ 3 kpc; it becomes supersonic at a distance of ~ 20 kpc, and speeds up to a velocity of ~ 400 km s^{-1} several hundred kiloparsecs away. The external pressure of the intergalactic gas produces a shock wave at a distance of ~ 300 kpc. In this model, the diffusion coefficient of particles is not given independently and is consistently calculated, being dependent on the power of sources and the spectrum of accelerated particles. Remarkably, the obtained transport coefficients and other model parameters are consistent with the empirical diffusion model for cosmic ray propagation in the version with the galactic wind [7, 13].

5. Cosmic rays in supernova remnants

There are a lot of observations evidencing the presence of relativistic particles in shell-like supernova remnants. The results of the observations can be summarized briefly as follows.

(1) Supernova remnants are sources of synchrotron radio emission which suggests the presence of relativistic electrons there with a total energy of $10^{48} - 10^{49}$ erg and the spectrum $E^{-1.9} - E^{-2.5}$ in the particle energy range 50 MeV – 30 GeV [6, 50, 51]. This is sufficient to provide the electron density observed in cosmic rays, assuming a galactic supernova explosion rate of $\nu_{\rm sn} \sim 1/30$ y^{-1}.

(2) Synchrotron emission in the X-ray range up to several keV was established first for SN 1006 [52] and then for other young supernova remnants with ages of 300–2000 years, including Cas A, RX J1713.7-3946, RX J0852-46, Tycho, RCW 86, and Kepler, suggesting the presence of electrons with energies up to $\sim 10^{13}$ eV and possibly higher. The emission is generated in a narrow region immediately behind the shock front, in which downstream electrons, accelerated at the front, lose energy via synchrotron radiation. The size of the emission region enables determination of the magnetic field intensity, which turns out to be quite significant up to several hundred microgauss (see Ref. [53]).

(3) The presence of the proton-nuclear component of cosmic rays can in principal be established from gamma-ray emission of supernova remnants, originated in the process $pp \to \pi^0 \to \gamma\gamma$ which is effective in relatively high-density

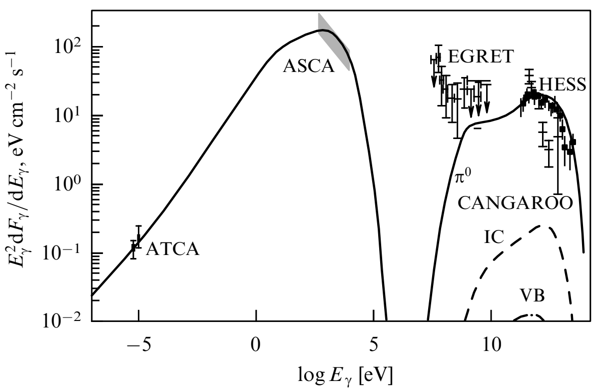

Figure 3. The emission spectrum of the supernova RX J1713.7-3946 remnant and its modeling [62]; F_γ is the photon flux in units [cm^{-2} s^{-1} eV^{-1}]. The results of calculations for the synchrotron radiation and gamma-ray emission due to π^0-decays are shown by solid lines; the dashed line depicts the contribution from the Compton scattering (IC), the dash-dotted line involves the bremsstrahlung radiation (VB). (ATCA: Australia Telescope Compact Array, ASCA: Advanced Satellite for Cosmology and Astrophysics, CANGAROO: Collaboration of Australia and Nippon for a Gamma-Ray Observatory in the Outback, and HESS: High Energy Stereoscopic System.)

regions. The analysis of the EGRET data for gamma-photon energies of 30 MeV – 30 GeV indicates the presence of the expected excess of the emission from several extended supernova remnants, including γ Cygni, IC433, and Monoceros [54, 55]. Testing this result is expected from the GLAST mission.

(4) In about the last five years, reliable evidence has appeared on TeV gamma-ray emission from the shells of young supernova RX J1713.7-3946 [56 – 58], Cas A [59], RX J0852-46 [60] remnants, and approximately three other supernova remnants (their identification is not always unique), which were detected in the course of the galactic plane survey for $-30^\circ < l < 30^\circ$ carried out by the HESS (High Energy Stereoscopic System) experiment [61], which registers Cherenkov atmospheric emission. The emission spectrum is close to E^{-2}, with the maximum photon energy detected reaching ~ 40 TeV. Most likely, the emission is produced by protons and nuclei accelerated up to energies $E \sim 5 \times 10^{14}$ eV per nucleon (see the discussion in Refs [56 – 62]). Electrons can also be the source of TeV photons through Compton up-scattering of the background radiation, but this mechanism requires comparatively low values of the magnetic field within the limits 10 – 30 μG (the field value is determined from the ratio of the Compton-to-synchrotron emission fluxes), which generally is not supported by observational data. Paper [61] concludes that observations of TeV emission from shell-like supernova remnants suggest that around 20% of kinetic energy of the expanding supernova shell is, on average, transferred to the proton-nuclear component of cosmic rays and that supernova remnants can produce this radiation for about 10^4 years. This conclusion supports the idea that supernova remnants are the principal sources of cosmic rays in the Galaxy.

Figure 3 shows an example of calculations of the emission from a supernova remnant in the entire range of the electromagnetic spectrum. The calculations were carried out in paper [62] for the source RX J1713.7-3946. It should be noted that the density ratio of the accelerated electrons to protons required by this simulation turns out to be an order of magnitude smaller than the directly observed cosmic ray value $\sim 1-2\%$ at an energy of 1 GeV.

6. Particle acceleration in supernova remnants

Let us now discuss the cosmic ray acceleration mechanism in supernova remnants, which is a version of the first-order Fermi acceleration [63]. The acceleration occurs in the shock-compressed gas stream due to numerous intersections of the shock front by rapid diffusing particles [64, 65] (see also reviews in Ref. [9]). The momentum distribution of particles has the form $N(p) \sim p^{-(r+2)/(r-1)}$, where r is the gas compression in the shock, so that $N(p) \sim p^{-2}$ for the maximum compression $r = 4$ of ideal monatomic gas in the strong shock without radiation loss. The acceleration turns out to be quite significant and for large Mach numbers of the shock wave, $M \gg 1$, the pressure of accelerated particles at the shock front reaches the values of $P_{\rm cr} = \xi_{\rm cr} \rho u_{\rm sh}^2$, where $\xi_{\rm cr} \sim 0.5$ [66] (here, ρ is the interstellar gas density, and $u_{\rm sh}$ is the shock front velocity). Such a high efficiency of the acceleration modifies the shock wave profile due to cosmic ray pressure. As a result, the spectrum of accelerated particles at very high energies becomes more flat (hard) than p^{-2}, and for energies below several GeV per nucleon, just the opposite, it becomes more steep.

To accelerate particles on a spherical shock front with radius $R_{\rm sh}$, the following condition must be satisfied:

$$D(p) \leqslant 0.1 u_{\rm sh} R_{\rm sh} , \tag{6}$$

where the numerical value of the factor on the right-hand side is approximate.

The maximum value in the r.h.s. of relation (6), which is on the order of $10^{28} (W_{51}/n)^{2/5}$ [cm^2 s^{-1}], is attained at the beginning of the Sedov stage of the evolution of the shock generated by a supernova explosion with the kinetic energy $W = 10^{51} W_{51}$ [erg] in the interstellar medium with the density n [cm^{-3}]. The standard diffusion coefficient (1) or (2) of cosmic rays in the interstellar medium is too high to provide the acceleration. The necessary anomalously low value of the diffusion coefficient can be self-consistently provided by accelerated particles themselves due to the stream instability in the shock wave precursor which has the characteristic size $D(p)/u_{\rm sh}$ [65, 67]. The Bohm limit in the interstellar magnetic field, $D = D_{\rm B} = v r_{\rm g}/3$, which assumes a random field amplification up to the values of $\delta B \approx B_{\rm ism}$ on scales necessary for the resonance scattering of particles, has been used for a long time as the most optimistic estimate for the diffusion coefficient appearing in this way. Then, formula (6) gives the estimate $E_{\max} \approx 10^{14} Z$ [eV] of the maximal energy of accelerated particles at the beginning of the Sedov stage and yields weak dependence $E_{\max} \sim t^{-1/5}$ at later times. Under these assumptions, numerical modeling of cosmic ray acceleration and the supernova remnant evolution have been carried out [66, 68].

The development of the theory of strong stream instability in the shock wave precursor [69 – 72] has shown that the use of the Bohm acceleration limit in the interstellar magnetic field is incorrect. For $u_{\rm sh} \gg 10^3$ km s^{-1}, random fields are amplified up to the level $\delta B \gg B_{\rm ism}$, and for $u_{\rm sh} < 10^3$ km s^{-1} random fields $\delta B < B_{\rm ism}$ and rapidly decrease with supernova remnant age due to turbulence dissipation. According to estimates [70], in extreme conditions, which apparently can be realized at the initial stage of shell expansion in supernovae SN Ib/c (SN1998 bw, for example), the random field can be as high as

$$\delta B_{\max} \sim 10^3 \, \frac{u_{\rm sh}}{3\times 10^4 \text{ km s}^{-1}} \, n^{1/2} \; [\mu\text{G}] \,, \tag{7}$$

and the maximal energy of accelerated particles can reach

$$E_{\max} \sim 10^{17} Z \, \frac{u_{\rm sh}}{3\times 10^4 \text{ km}^2 \text{ s}^{-2}} \, \frac{\xi_{\rm cr}}{0.5} \, M_{\rm ej}^{1/3} n^{1/6} \; [\text{eV}] \tag{8}$$

(here, $M_{\rm ej}$ is the mass of the ejecta measured in solar masses). As was pointed out in Section 5, the presence of a strong magnetic field is confirmed by X-ray observations of young supernova remnants. A very strong field amplification in young supernova remnants is indirect evidence of the acceleration of protons, which is accompanied by a strong stream instability. The predicted strong dependence $E_{\max}(t)$ allows one to understand why TeV gamma-ray emission is observed only from young supernova remnants.

The theoretical spectrum of the sources of galactic cosmic rays was computed in Ref. [72] by means of averaging the spectrum of particles accelerated and injected into the interstellar medium during the supernova remnant lifetime. The averaged source of high-energy protons turned out to have a power-law energy spectrum with a sharp kink near $E_{\rm k}$ close to the energy of the bend:

$$Q \sim \xi_{\rm cr} v_{\rm sn} W E^{-2} \quad \text{for} \quad E \leqslant E_{\rm k} \,, \tag{9}$$

where $E_{\rm k} = 4\times 10^{15} (\xi_{\rm cr}/0.5) W_{51} M_{\rm ej}^{-2/3} n^{1/6}$ [eV], and

$$Q \sim E^{-s} \quad \text{for} \quad E > E_{\rm k} \,, \tag{10}$$

where $s = 3.5-5$ in different variants of the model. Particles with energies $E < E_{\rm k}$ are accelerated at the Sedov stage; particles with energies $E > E_{\rm k}$ are accelerated at the earlier stage of free expansion when the maximum energy of individual particles is high but the total number of accelerated particles is relatively small, which explains the steep form of the spectrum. For each type of ions, the break appears at the energy $ZE_{\rm k}$ proportional to the charge. These results are basically consistent with observations of the spectrum and composition of cosmic rays [73] and apparently explain the presence of the knee in the spectrum of all particles at an energy of 3×10^{15} eV. To refine the theory, a population analysis taking into account the dispersion of parameters entering formula (9) is needed (see Ref. [74]).

7. Ultrahigh energies

The statement that the density of cosmic rays in the intergalactic space is relatively small as compared to the galactic one relates to particles with not too high an energy, which are effectively accelerated in the galactic sources and are well confined in the galactic magnetic fields. The observed cosmic rays with the highest energies, which apparently have extragalactic origin, are more homogeneously distributed in the Universe. The spectrum of particles with energies exceeding 10^{17} eV as obtained in the HiRes experiment (High Resolution Fly's Eye) is shown in Fig. 4. The sharp flux decrease for $E > 6\times 10^{19}$ eV evidences the presence of the blackbody spectral cut-off predicted in papers [76, 77], which is caused by the photopion energy loss in a time on the order of about 4×10^9 years due to the interaction of particles (protons) with cosmic microwave background photons. At proton energies 3×10^{20} eV, the characteristic time of energy losses amounts to $\sim 10^8$ years, so these particles can reach the

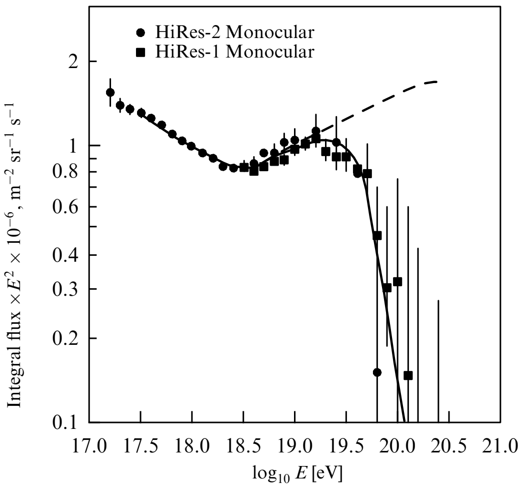

Figure 4. Spectrum of ultrahigh-energy cosmic rays according to the HiRes data [75]. The curves show the presence of the spectral cut-off at an energy of 6×10^{19} eV.

Earth from comparatively small cosmological distances. Possible sources of the ultrahigh energy particles could in principle include active galactic nuclei, interacting galaxies, gamma-ray bursts and some others (see review [78]).

When interpreting the observed spectrum of ultrahigh energy particles two main versions are considered. According to the first version, the flattening of the spectrum at an energy of 4×10^{18} eV (see Fig. 4) is explained as the passage from galactic to extragalactic cosmic rays (see Refs [79, 80] for more detail). Here, the spectrum of extragalactic sources is close to $E^{-2.3}$ and their composition is mixed; more precisely, in the extragalactic sources protons and heavy nuclei are presented in the normal proportion. In another version [81], the passage from galactic to extragalactic cosmic rays in the observed spectrum occurs at energy $\sim 10^{18}$ eV. In the last case, the spectrum of the sources is close to $E^{-2.7}$, and for a purely proton composition the feature at $E \sim 4\times 10^{18}$ eV is explained as being due to the contribution to the total energy loss by the microwave background radiation from pair creation. The choice between these alternatives can be made after having measured more accurately the particle composition for energies $E \gtrsim 10^{18}$ eV (see a detailed discussion in Ref. [80]). In any case, it is required that galactic sources accelerate particles up to $E \sim 10^{18}-10^{19}$ eV, which significantly exceeds estimates made in Section 6. Perhaps this issue can be solved by taking into account the contribution from rare hypernovae with a huge energy release, $W \approx 3\times 10^{52}$ erg [74]. Another possibility is related to a strong additional acceleration of particles by an ensemble of shocks in O-B star associations [82] or in the galactic wind [83]. The contribution from young neutron stars with a high magnetic field ($\geqslant 10^{13}$ G) and relativistic wind, in which ion acceleration up to $E \sim 10^{20}$ eV is principally possible, is not excluded, either [84].

In general, the main attention in present-day cosmic ray studies is focused on the high-energy region. Clearly understanding the nature of the knee in the particle spectrum at $E \approx 3\times 10^{15}$ eV (notice that this feature was experimentally discovered almost 50 years ago [85]), determining the particle acceleration limit in the Galaxy, and analyzing ultrahigh-energy particle acceleration in extragalactic sources are required.

References

1. Gaisser T K, in *Energy Budget in the High Energy Universe*: *Proc. of the Intern. Workshop, Kashiwa, Japan, 22–24 February 2006* (Eds K Sato, J Hisano) (Singapore: World Scientific, 2007); astro-ph/0608553
2. Ginzburg V L *Dokl. Akad. Nauk SSSR* **76** 377 (1951)
3. Ginzburg V L *Dokl. Akad. Nauk SSSR* **92** 1133 (1953)
4. Ginzburg V L *Usp. Fiz. Nauk* **51** 343 (1953)
5. Ginzburg V L *Annu. Rev. Astron. Astrophys.* **28** 1 (1990)
6. Ginzburg V L, Syrovatskii S I *Proiskhozhdenie Kosmicheskikh Luchei* (The Origin of Cosmic Rays) (Moscow: Izd. AN SSSR, 1963) [Translated into English (Oxford: Pergamon Press, 1964)]
7. Berezinskii V S, Bulanov S V, Ginzburg V L, Dogel V A, Ptuskin V S *Astrofizika Kosmicheskikh Luchei* (Astrophysics of Cosmic Rays) 2nd ed. (Ed. V L Ginzburg) (Moscow: Nauka, 1990) [Translated into English (Amsterdam: North-Holland, 1990)]
8. Ginzburg V L *Usp. Fiz. Nauk* **166** 169 (1996) [*Phys. Usp.* **39** 155 (1996)]
9. *Space Sci. Rev.* **99** 1–373 (2001)
10. McDonald F B, Ptuskin V S, in *The Century of Space Science* (Eds J A M Bleeker, J Geiss, M C E Huber) (Dordrecht: Kluwer Acad. Publ., 2001) p. 677
11. Ginzburg V L, Ptuskin V S *Usp. Fiz. Nauk* **117** 585 (1975) [*Sov. Phys. Usp.* **18** 931 (1975)]; *Rev. Mod. Phys.* **48** 161 (1976)
12. Ginzburg V L, Khazan Ia M, Ptuskin V S *Astrophys. Space Sci.* **68** 295 (1980)
13. Bloemen J B G M et al. *Astron. Astrophys.* **267** 372 (1993)
14. Ptuskin V S, Soutoul A *Astron. Astrophys.* **337** 859 (1998)
15. Strong A W, Moskalenko I V *Astrophys. J.* **509** 212 (1998)
16. Ptuskin V S et al. *Astrophys. J.* **642** 902 (2006)
17. Ptuskin V S, Zirakashvili V N *Adv. Space Res.* **37** 1898 (2006)
18. Hunter S D et al. (EGRET Collab.) *Astrophys. J.* **481** 205 (1997)
19. Strong A W, Moskalenko I V, Reimer O *Astrophys. J.* **613** 962 (2004)
20. Breitschwerdt D, Dogiel V A, Völk H J *Astron. Astrophys.* **385** 216 (2002)
21. Pohl M, Esposito J A *Astrophys. J.* **507** 327 (1998)
22. Berezhko E G, Völk H J *Astrophys. J.* **611** 12 (2004)
23. de Boer W et al. *Astron. Astrophys.* **444** 51 (2005)
24. Atkins R et al. (Milagro Collab.) *Phys. Rev. Lett.* **95** 251103 (2005)
25. Prodanović T, Fields B D, Beacom J F *Astropart. Phys.* **27** 10 (2007); astro-ph/0603618
26. Sreekumar P et al. *Phys. Rev. Lett.* **70** 127 (1993)
27. Ginzburg V L *Nature Phys. Sci.* **239** 8 (1972)
28. Ginzburg V L, Ozernoi L M *Astron. Zh.* **42** 943 (1965) [*Sov. Astron.* **9** 726 (1965)]
29. Samui S, Subramanian K, Srianand R, astro-ph/0505590
30. Toptygin I N *Kosmicheskie Luchi v Mezhplanetnykh Magnitnykh Polyakh* (Cosmic Rays in the Interplanetary Magnetic Fields) (Moscow: Nauka, 1983)
31. Chuvilgin L G, Ptuskin V S *Astron. Astrophys.* **279** 278 (1993)
32. Casse F, Lemoine M, Pelletier G *Phys. Rev. D* **65** 023002 (2001)
33. Elmegreen B G, Scalo J *Annu. Rev. Astron. Astrophys.* **42** 211 (2004)
34. Goldreich P, Sridhar S *Astrophys. J.* **438** 763 (1995)
35. Yan H, Lazarian A *Astrophys. J.* **614** 757 (2004)
36. Syrovatskii S I *Comm. Astrophys. Space Phys.* **3** 155 (1971)
37. Ptuskin V S et al. *Astron. Astrophys.* **268** 726 (1993)
38. Hörandel J R, Kalmykov N N, Timokhin A V *Astropart. Phys.* **27** 119 (2007); astro-ph/0609490
39. Ginzburg V L *Astron. Zh.* **42** 1129 (1965) [*Sov. Astron.* **9** 877 (1965)]
40. Ginzburg V L, Ptuskin V S, Tsytovich V N *Astrophys. Space Sci.* **21** 13 (1973)
41. Dogiel V A, Gurevich A V, Zybin K P *Astron. Astrophys.* **281** 937 (1994)
42. Zweibel E G *Astrophys. J.* **587** 625 (2003)
43. Farmer A J, Goldreich P *Astrophys. J.* **604** 671 (2004)
44. Pikel'ner S B *Dokl. Akad. Nauk SSSR* **88** 229 (1953)
45. Parker E N *Astrophys. J.* **145** 811 (1966)
46. Kuznetsov V D, Ptuskin V S *Pis'ma Astron. Zh.* **9** 138 (1983) [*Sov. Astron. Lett.* **9** 75 (1983)]
47. Parker E N *Astrophys. J.* **401** 137 (1992)
48. Zirakashvili V N et al. *Astron. Astrophys.* **311** 113 (1996)
49. Ptuskin V S et al. *Astron. Astrophys.* **321** 434 (1997)
50. Shklovskii I S *Sverkhnovye Zvezdy i Svyazannye s Nimi Problemy* (Supernova Stars and Related Problems) 2nd ed. (Moscow: Nauka, 1976)
51. Lozinskaya T A *Sverkhnovye Zvezdy i Zvezdnyi Veter*: *Vzaimodeistvie s Gazom Galaktiki* (Supernovae and Stellar Wind: Interaction with Galactic Gas) (Moscow: Nauka, 1986) [Translated into English: *Supernovae and Stellar Wind in the Interstellar Medium* (New York: American Inst. of Phys., 1992)]
52. Koyama K et al. *Nature* **378** 255 (1995)
53. Völk H J, Berezhko E G, Ksenofontov L T *Astron. Astrophys.* **433** 229 (2005)
54. Esposito J A et al. *Astrophys. J.* **461** 820 (1996)
55. Sturner S J, Dermer C D *Astron. Astrophys.* **293** L17 (1995)
56. Muraishi H et al. (CANGAROO Collab.) *Astron. Astrophys.* **354** L57 (2000)
57. Enomoto R et al. (CANGAROO Collab.) *Nature* **416** 823 (2002)
58. Aharonian F A et al. (HESS Collab.) *Nature* **432** 75 (2004)
59. Aharonian F et al. (HESS Collab.) *Astron. Astrophys.* **370** 112 (2001)
60. Aharonian F et al. (HESS Collab.) *Astron. Astrophys.* **437** L7 (2005)
61. Aharonian F et al. (HESS Collab.) *Astrophys. J.* **636** 777 (2006)
62. Berezhko E G, Völk H J *Astron. Astrophys.* **451** 981 (2006); astro-ph/0602177
63. Fermi E *Phys. Rev.* **75** 1169 (1949)
64. Krymskii G F *Dokl. Akad. Nauk SSSR* **234** 1306 (1977) [*Sov. Phys. Dokl.* **22** 327 (1977)]
65. Bell A R *Mon. Not. R. Astron. Soc.* **182** 147 (1978)
66. Berezhko E G, Elshin V K, Ksenofontov L T *Zh. Eksp. Teor. Fiz.* **109** 3 (1996) [*JETP* **82** 1 (1996)]
67. Lagage P O, Cesarsky C J *Astron. Astrophys.* **118** 223 (1983)
68. Kang H, Jones T W *Astropart. Phys.* **25** 246 (2006)
69. Bell A R, Lucek S G *Mon. Not. R. Astron. Soc.* **321** 433 (2001)
70. Ptuskin V S, Zirakashvili V N *Astron. Astrophys.* **403** 1 (2003)
71. Bell A R *Mon. Not. R. Astron. Soc.* **353** 550 (2004)
72. Ptuskin V S, Zirakashvili V N *Astron. Astrophys.* **429** 755 (2005)
73. Hörandel J R *Astropart. Phys.* **19** 193 (2003)
74. Sveshnikova L G *Pis'ma Astron. Zh.* **30** 47 (2004) [*Astron. Lett.* **30** 41 (2004)]
75. Bergman D R (HiRes Collab.) *Nucl. Phys. B*: *Proc. Suppl.* **165** 19 (2007); astro-ph/0609453
76. Greisen K *Phys. Rev. Lett.* **16** 748 (1966)
77. Zatsepin G T, Kuz'min V A *Pis'ma Zh. Eksp. Teor. Fiz.* **4** 114 (1966) [*JETP Lett.* **4** 78 (1966)]
78. Torres D F, Anchordoqui L A *Rep. Prog. Phys.* **67** 1663 (2004)
79. Allard D, Parizot E, Olinto A V *Astropart. Phys.* **27** 61 (2007); astro-ph/0512345
80. Hillas A M, in *Cosmology, Galaxy Formation and Astroparticle Physics on the Pathway to the SKA* (Eds H-R Klockner et al.) (Oxford, 2006) (in press); astro-ph/0607109
81. Berezinsky V, Gazizov A Z, Grigorieva S I *Phys. Lett. B* **612** 147 (2005)
82. Bykov A M, Toptygin I M *Pis'ma Astron. Zh.* **27** 735 (2001) [*Astron. Lett.* **27** 625 (2001)]
83. Völk H J, Zirakashvili V N *Astron. Astrophys.* **417** 807 (2004)
84. Blasi P, Epstein R I, Olinto A V *Astrophys. J.* **533** L123 (2000)
85. Kulikov G V, Khristiansen G B *Zh. Eksp. Teor. Fiz.* **35** 635 (1958) [*Sov. Phys. JETP* **8** 441 (1959)]

PACS numbers: 74.20.De, 74.20.Mn, **74.72.–h**
DOI: 10.1070/PU2007v050n05ABEH006223

Ginzburg – Landau equations for high-temperature superconductors

V I Belyavsky, Yu V Kopaev

The phenomenological theory of superconductivity [1] formulated by V L Ginzburg and L D Landau in 1950 (long before the appearance of the Bardeen – Cooper – Schrieffer

(BCS) microscopic theory of superconductivity [2]) predetermined many prospective directions in condensed state physics. The complex order parameter introduced in paper [1] made it possible to describe the transition to the superconducting state as the establishment of phase coherence in an electronic system, while taking account of the gradient contribution to the free energy functional (in the spirit of Ornstein and Zernicke fluctuation theory) allowed consideration of the behavior of a superconducting system in inhomogeneous external fields, in particular, the Meissner effect. Such parameters of the Ginzburg – Landau theory as the coherence length and the penetration depth permitted seeing the difference in the behavior of different superconductors and making their simple classification (type I and type II superconductors [3]). The Ginzburg – Landau equations (derived in 1958 by L P Gor'kov [4] proceeding from the microscopic theory) are the principal instrument for interpretation of experimental data and underlie numerous technical applications.

The 1986 discovery of high-temperature superconductivity [5] and the consequent active experimental and theoretical studies of this unique phenomenon (following the way largely paved by the group of theoreticians headed by Ginzburg [6]) led to the necessity of explaining the properties of new superconductors that did not fit in the usual BCS scheme.

Ginzburg was one of the first to pay attention to the then unknown temperature range lying above the superconducting transition temperature T_c, in which strong fluctuation effects show themselves [7]. It is currently believed that the understanding of the nature of this region of the pseudogap state of high-temperature superconducting (HTSC) cuprates can provide insight into the microscopic mechanism of the superconductivity of these compounds.

Ginzburg's interest in the thermoelectric phenomena in superconductors [8] and in the giant diamagnetism of ordered states with orbital currents [9], which he has shown for over half a century, is now shared by many research workers in connection with the observed anomalous Nernst effect [10 – 12] and the nonlinear-in-field diamagnetism [13] in the region of the strong pseudogap of HTSC cuprates.

To explain the whole set of HTSC cuprate properties in both pseudogap and superconducting states, various theoretical schemes have been proposed, which are mostly based on the assumption that these properties are basically determined by strong electron correlations in copper – oxygen planes [14].

The Coulomb repulsion restricting the double occupation of the copper atom lattice sites in cuprate planes leads to the fact that the parent compound appears to be an antiferromagnetic (AF) insulator. With increasing concentration of carriers incorporated through doping, the long-range AF order is replaced by the short-range order, and the dielectric gap is preserved, thus offering the conditions for the occurrence of superconductivity with an unusual energy-gap symmetry [15]. Hence, strong Coulomb correlations lead not only to a rise of insulating state, but also to cuprate superconductivity.

The possibility of the occurrence of superconductivity in pairing repulsion, first noticed by Landau, was investigated by Kohn and Luttinger [16] for an isotropic degenerate electron gas, and by Moskalenko [17] and Suhl et al. [18] for metals with a two-band electronic spectrum. The estimates obtained in these works lead to rather low T_c values.

Here, we present the phenomenology of large-momentum superconducting pairing during Coulomb repulsion in the framework of the Ginzburg – Landau scheme and consider its application to the interpretation of the phase diagram of doped cuprate compounds.

For finite sections of the Fermi contour in the form of a rounded-corner square [19], which is typical of cuprates, the nesting condition

$$\varepsilon(\mathbf{Q}+\mathbf{p})+\varepsilon(\mathbf{p})=2\mu \tag{1}$$

holds true, where $\varepsilon(\mathbf{p})$ is the dispersion law, and μ is the chemical potential, which leads to dielectric instability of the system. The momentum $\mathbf{Q}$ determines the period of state with a long-range dielectric order. Furthermore, for finite sections of the Fermi contour the mirror nesting condition [20]

$$\varepsilon\left(\frac{\mathbf{K}}{2}+\mathbf{k}\right)=\varepsilon\left(\frac{\mathbf{K}}{2}-\mathbf{k}\right) \tag{2}$$

is fulfilled, which corresponds to the fact that a pair of likely charged particles with momenta $\mathbf{k}_{\pm}=\mathbf{K}/2\pm\mathbf{k}$ belonging to the Fermi contour has the total momentum $\mathbf{K}$ when the momentum $\mathbf{k}$ of the relative motion is determined in a certain part of the Brillouin zone (the kinematically restricted region). The mirror nesting produces instability with respect to singlet superconducting pairing with pair momentum $\mathbf{K}$.

The nesting and mirror nesting of the Fermi contour make possible the development of instability in both the superconducting and a certain insulating channel of pairing upon Coulomb repulsion. In the insulating channel no logarithmic singularity is induced by the mirror nesting which (as distinct from the ordinary nesting) cannot therefore be the reason for a radical transformation of the phonon spectrum.

An approximate mirror nesting takes place in only finite sections of the Fermi contour, and hence the finite density of noncondensate particles is retained up to $T=0$, which is reflected in Drude type behavior of optical conductivity [21] and a quasilinear temperature dependence of heat capacity [22] of cuprates in the superconducting state.

The characteristic form of the superconducting region in the phase diagram of cuprates is determined by two competing factors: with increased doping, the momentum space area making an effective contribution to the order parameter increases, while the length of the Fermi contour sections with mirror nesting decreases. An approximate mirror nesting can lead to superconductivity with large (but generally incommensurate) pair momentum. A further evolution of the Fermi contour with doping [23] makes the channel of pairing with large momentum ineffective. The usual channel of Cooper pairing with zero pair momentum in the electron – phonon interaction (EPI) may also turn out to be ineffective because of the smallness of the Tolmachev logarithm which restricts the coupling constant from below.

Apart from the spin antiferromagnetic and superconducting states with a long-range order, the phase diagram of cuprates with hole doping shows a pseudogap state restricted from above by a certain temperature T^*. The fact that some phase transition corresponds to this temperature has no convincing experimental confirmation, which gives grounds for treating T^* as the temperature of crossover between the pseudogap states for $T_c<T<T^*$ and the normal Fermi liquid for $T>T^*$. The pseudogap behavior can be associated with the insulating short-range order [24] or with the developed fluctuations of the superconducting order parameter for $T>T_c$, which appears possible for a low superfluid density (a low phase stiffness), for which reason the loss of phase coherence occurs earlier than the pair-break of the Cooper pair [25]. In this case, incoherent pairs (a fluctuating superconducting order) can exist in a certain temperature range above T_c. The characteristic width of this interval has the order of T_c and proves to be much lower than T^* in underdoped compounds.

If, as is assumed in Ref. [26], the pseudogap manifests a hidden (hardly detectable) long-range dielectric antiferromagnetic order in the form of a density wave of orbital current with d-wave symmetry, then T^* has the meaning of phase transition temperature. The orbital antiferromagnetism possibly manifests itself as only the short-range order [27], in particular, as the insulating state of the Abrikosov vortex core (which considerably lowers its energy and has an experimental confirmation [28]).

The pseudogap region can conditionally be divided into the regions of a strong pseudogap for $T_c < T < T^*_{str}$, in which the developed fluctuations of the superconducting order parameter induce an increase in the diamagnetic response and a giant Nernst effect, and a weak pseudogap for $T^*_{str} < T < T^*$ with anomalies of some physical properties. The upper boundary T^*_{str} of the strong pseudogap is the temperature of crossover between the regions of weak and developed fluctuations of the superconducting order parameter.

In the scheme of large-momentum pairing, the screened Coulomb repulsion, as distinct from the pairing attraction, allows not only the bound state, but also the long-lived quasistationary states of incoherent pairs [29], which broaden substantially the region of developed fluctuations of the superconducting order parameter at temperatures above T_c and can be associated with the state of the strong pseudogap.

The hidden long-range order in the form of a current-density wave with d-wave symmetry can manifest itself in the relative phase of two components of the superconducting order parameter [31, 32]. The zeros of the superconducting (for extended s-wave symmetry) and orbital antiferromagnetic (corresponding, according to Ref. [26], to the flux-phase [27] possessing d-wave symmetry) order parameters do not coincide, which can be associated with the relative insensitivity of cuprate superconductivity to scattering by nonmagnetic impurities.

The necessary (and sufficient in the case of mirror nesting) condition of superconductivity under repulsion is the existence of at least one negative eigenvalue of the pairing interaction operator. The eigenfunction corresponding to the negative eigenvalue has the line of zeros crossing the Fermi contour in the domain of kinematic constraint. The superconducting energy gap appears to be a function with alternating signs of momentum of the relative motion of a pair inside this region, which vanishes at several points of the Fermi contour [20].

The kinematic constraint is sufficient for one negative eigenvalue to separate from the spectrum of the kernel of the screened Coulomb pairing interaction [33]. Such pairing interaction can approximately be described by a degenerate kernel with two even (with respect to the transformation $\mathbf{k} \to -\mathbf{k}$) eigenfunctions with eigenvalues of opposite signs. Thus, the superconducting ordering upon pairing Coulomb repulsion corresponds to a two-component complex order parameter (conventional superconductivity upon pairing attraction due to EPI is described by a one-component order parameter).

Pairing repulsion leads to the existence of three singular lines with common intersection points in each domain of kinematic constraint corresponding to one of the crystal equivalent pair momenta. One of these lines is part of the Fermi contour on which the pair kinetic energy

$$2\xi(\mathbf{k}) = \varepsilon\left(\frac{\mathbf{K}}{2} + \mathbf{k}\right) + \varepsilon\left(\frac{\mathbf{K}}{2} - \mathbf{k}\right) - 2\mu$$

vanishes because of the mirror nesting (when crossing this line the quasiparticle charge reverses sign). The second singular line is the line of zeros of the order parameter (the intersection points of this line with the Fermi contour correspond to a gapless spectrum of quasiparticles). The group velocity of the quasiparticle vanishes in the line of minima of the quasiparticle energy as a function of momentum [20]. The coherence factors exhibit a nontrivial dependence on the momentum with inhomogeneous distribution of particles in momentum space, which leads to asymmetry of tunnel conductivity, to a peak-dip-hump structure of tunnel and photoemission spectra, and also to a restriction of Andreev reflection in cuprates [20]. The transition to a superconducting state causes a shift (linear in the absolute value of the order parameter) in the chemical potential depending on the ratio of areas of the occupied and vacant parts of the domain of kinematic constraint [34].

In each domain of kinematic constraint one can determine the order parameter in the form of the product of wave functions of the relative motion and free motion of the center-of-mass of a pair with momentum $\mathbf{K}_j$ and radius vector $\mathbf{R}$. In the mean-field approximation, the wave function $\Psi_j(\mathbf{k})$ of the relative motion is proportional to the nontrivial solution of the self-consistent equation. With allowance for the degeneracy due to crystal symmetry, the order parameter is written down as

$$\Psi(\mathbf{R}, \mathbf{k}) = \sum_j \gamma_j \exp(\mathrm{i}\mathbf{K}_j\mathbf{R})\,\Psi_j(\mathbf{k}), \quad (3)$$

where the domain of definition of momentum $\mathbf{k}$ of the relative motion is the union of all the domains of kinematic constraint, and the coefficients γ_j are determined by the interaction removing the degeneracy typical of pairing with large momentum.

Under dominating EPI-induced attraction, which itself can lead to conventional s-wave superconductivity, all the coefficients γ_j prove to be identical. The function $\Psi_j(\mathbf{k})$ has a line of zeros crossing the Fermi contour in the corresponding domain of kinematic constraint, so that the order parameter has zeros on the Fermi contour (distributed symmetrically about quadrants of the Brillouin zone) and remains invariant under rotation through the angle $\pi/2$ in momentum space. Such order parameter corresponds to extended s-wave symmetry.

The scheme of large-momentum pairing with allowance made for the contribution of the EPI mechanism of pairing [35] provides an explanation of the occurrence of the isotope effect in cuprates, including the negative isotope effect [36].

If the dominating pairing perturbation is the exchange by AF magnons [37, 38], the coefficients γ_j corresponding to neighboring Ξ_j regions have different signs. In this case, when turning through the angle $\pi/2$, the order parameter changes sign and four more zeros are added to the zeros due to pairing repulsion at the intersection points of the Fermi contour with the diagonals of the Brillouin zone. Then, the order parameter can be attributed to the extended d-wave symmetry. In different compounds (or in the bulk or the near-surface layer of one compound) both types of symmetry show themselves [39, 40].

The expansion of the order parameter in terms of the complete orthonormal system of two eigenfunctions $\varphi_s(\mathbf{k})$ of the degenerate kernel $U(\mathbf{k}-\mathbf{k}')$ of the pairing-interaction operator allows defining the order parameter by two of its complex components depending, in the case of a spatially inhomogeneous system, on the radius vector of the center of mass:

$$\Psi(\mathbf{R},\mathbf{k}) = \sum_{s=1}^{2} \Psi_s(\mathbf{R})\,\varphi_s(\mathbf{k})\,. \tag{4}$$

The whole dependence on the momentum of relative motion is transferred to the eigenfunctions defined without regard to the self-consistent equation.

The two-dimensional (calculated for one cuprate plane) free-energy density in the Ginzburg–Landau functional can be given as follows:

$$f = f_0 + f_{\mathrm{g}} + f_{\mathrm{m}}\,, \tag{5}$$

where f_0 are contributions of the second and fourth order in $\Psi_s(\mathbf{R})$, f_{g} is the gradient term, and f_{m} is the magnetic field energy density.

Expansion of the free-energy density in powers of the order parameter can generally be represented in the form

$$f_0 = \sum_{ss'} A_{ss'}\Psi_s^*\Psi_{s'} + \frac{1}{2}\sum_{ss'tt'} B_{ss'tt'}\Psi_s^*\Psi_{s'}^*\Psi_t\Psi_{t'}\,. \tag{6}$$

Here, the matrices $A_{ss'}$ and $B_{ss'tt'}$ are functions of temperature and doping.

Retaining in the gradient term only the contribution of the second-order in $\nabla\Psi_s$, which is sufficient for a slowly varying $\Psi_s(\mathbf{R})$, we can write the gradient term as

$$f_{\mathrm{g}} = \frac{\hbar^2}{4m}\sum_{ss'}[\widehat{D}\Psi_s]^{\dagger} M_{ss'}[\widehat{D}\Psi_{s'}]\,, \tag{7}$$

where the elements of the matrix $M_{ss'}$ also depend on the temperature and doping, and the covariant differentiation operator has the form

$$\widehat{D} = -\mathrm{i}\nabla - \frac{2e}{\hbar c}\,\mathbf{A}\,. \tag{8}$$

Here, $\mathbf{A} = \mathbf{A}(\mathbf{R})$ is the vector potential determining the induction of the magnetic field $\mathbf{B} = \mathrm{rot}\,\mathbf{A}$. Field $\mathbf{A}$ characterizes not only the external magnetic field, but also the internal magnetic field associated with the possible occurrence of spontaneous orbital currents.

The change of the two-dimensional density of the medium free energy in a magnetic field is written out as

$$f_{\mathrm{m}} = \frac{z_0}{8\pi}\,(\mathrm{rot}\,\mathbf{A})^2\,, \tag{9}$$

where z_0 is the distance between the neighboring planes.

The matrices determining the expansion of the free energy in power series of the order parameter were calculated in Ref. [41] in the weak coupling approximation.

The components of the order parameter have a common phase factor $\Psi_s = \psi_s \exp(\mathrm{i}\Phi)$. The phase Φ referring to the motion of the center of mass of pairs is associated with establishment of phase coherence in the system of pairs upon transition to the superconducting state. The complex coefficients ψ_s are characterized by the absolute values related to each other by the normalization condition $|\psi_1|^2 + |\psi_2|^2 = n_{\mathrm{sf}}/2$ and by the relative phase β: $\psi_2 = \psi_1 \exp(\mathrm{i}\beta)$. Thus, for a given superfluid density n_{sf}, the relative orbital motion of the pair is characterized by two independent parameters: by one of the modulus (ψ_1 or ψ_2), and by the relative phase β.

The occurrence of a nonzero modulus of the order parameter is associated with violation of gauge symmetry upon transition to the superconducting state, i.e., with the charge degree of freedom of a pair. It is natural to assume that the phase β, which shows up in the gradient term, is associated with the orbital current degree of freedom of the relative motion of the pair.

The state of a spatially homogeneous system is determined by the minimum condition of free-energy density (5). For a temperature of $T > T_{\mathrm{sc}}$, where T_{sc} is the superconducting phase transition temperature, the elements of the matrix $A_{ss'}$ are greater than zero, and the minimum of function (5) corresponds to the obvious trivial solution $\psi_1 = \psi_2 = 0$ with an indefinite relative phase β. For $T < T_{\mathrm{sc}}$, a nontrivial solution occurs for which the equilibrium values of ψ_1, ψ_2, and β are determined by the values of the matrices $A_{ss'}$ and $B_{ss'tt'}$.

For simplification, we can put $\psi_1 = \psi_2 \equiv \psi$. In the case of a spatially homogeneous system without an external magnetic field, the summands f_{g} and f_{m} are absent in expansion (5). The free-energy density can then be rewritten in the form

$$f_0 = a_1\psi^2 + \frac{1}{2}(B + 2C\cos\beta + D\cos^2\beta)\psi^4\,, \tag{10}$$

where $a_1 = A_{11} + A_{22}$, $B = B_{1111} + 2B_{1122} + B_{2222}$, $C = 2(B_{1112} + B_{1222})$, and $D = 4B_{1122}$. Notice that the simplest approximation corresponding to a symmetric occupation of the domain of kinematic constraint gives $B \neq 0$ and $C = D = 0$. Therefore, for the analysis of possible states in the phase diagram it is necessary to remove this restriction.

The study of function (10) for an extremum at $T < T_{\mathrm{sc}}$ reveals that the minimum is reached for $\beta = \pi$ and $\psi \neq 0$, when the condition $C \geqslant D$ holds true or for $\beta < \pi$ and $\psi \neq 0$ if $C \leqslant D$. In the latter case, the relative phase is determined by the relationship $\cos\beta = -C/D$. To distinguish between the two thermodynamically equilibrium SC phases, we shall introduce the order parameter $\alpha = \pi - \beta$. Thus, for $C \geqslant D$ we have $\alpha = 0$, while for $C < D$ we have $\alpha \neq 0$.

The deviation of the relative phase β from π permits an obvious interpretation. The change in the phase of the electron annihilation operator at the site of the crystal lattice $\mathbf{n}$ can be due to the vector potential $\mathbf{A}(\mathbf{n})$ of the magnetic field occurring with the appearance of the orbital antiferromagnetic (OAF) ordering [26]. In the superconducting state, the OAF ordering can appear as AF-correlated circulations of orbital currents [30] surviving also for $T > T_{\mathrm{sc}}$.

The occurrence of orbital currents in the superconducting state leads to the necessity of allowing for in the Ginzburg–Landau functional the contribution due to the energy of their magnetic field. This contribution is formally taken into account in the free-energy density by the term f_{m} if we understand $\mathbf{B}$ as magnetic induction of the field of orbital currents. A simple addition to f_0 of a summand of the form $f_{\mathrm{m}}(\alpha) = \varkappa\alpha^2$ with positive $\varkappa$ excludes the minimum of the free-energy density for $\alpha \neq 0$. This naturally necessitates a consideration of competition between two pairing channels:

the large-momentum superconducting pairing, and the insulating OAF pairing with the order parameter α.

Since spontaneous orbital currents can also occur in the absence of superconducting order, the free-energy density (in the absence of superconductivity) near an OAF transition may be represented as an expansion in even powers of α:

$$f_{\mathrm{d}} = a_2\alpha^2 + \frac{1}{2}\, b_2\alpha^4 , \tag{11}$$

where b_2 is a positive doping function, and the coefficient a_2 near the line of an insulating phase transition can be represented as $a_2 = \tau_2 a'$, where $a' > 0$ and $\tau_2 = \big(T - T_{\mathrm{d}}(x)\big)/T_{\mathrm{d}}(x)$, with $T_{\mathrm{d}}(x)$ being the temperature of transition into the OAF state.

The relation between the two types of ordering is determined by the gradient term f_{g} in which the contribution of spontaneous currents to the spatially homogeneous system should be retained. This leads to the appearance in the free energy of the summand $b_{12}\psi^2\alpha^2$, where b_{12} is a doping-dependent phenomenological parameter determined by the matrix $M_{ss'}$.

Thus, the free-energy density describing the competition between the superconducting and OAF-ordered states up to and including fourth-order terms assumes the form

$$f = a_1\psi^2 + a_2\alpha^2 + \frac{1}{2}\, b_1\psi^4 + b_{12}\psi^2\alpha^2 + \frac{1}{2}\, b_2\alpha^4 , \tag{12}$$

where the coefficient b_1, as can be seen from expression (10), is determined by the nonzero elements of the matrix $B_{ss'tt'}$. The expansion (12) makes sense only in a small neighborhood of both phase transitions, where the lines $T_{\mathrm{sc}}(x)$ and $T_{\mathrm{d}}(x)$ either intersect or run near each other.

Doping causes the suppression of orbital antiferromagnetism and it is therefore natural to assume $T_{\mathrm{d}}(x)$ and $T_{\mathrm{sc}}(x)$ to be decreasing functions of doping. Suppose that for small x the insulating order with the transition temperature $T_{\mathrm{d}}(x)$ dominates over superconductivity with the transition temperature $T_{\mathrm{sc}}(x)$ and is quickly suppressed by doping. This implies the possibility for the lines $T_{\mathrm{d}}(x)$ and $T_{\mathrm{sc}}(x)$ to intersect at a certain point (a tetracritical point c) corresponding to the doping x_0.

Minimization of function (12) gives rise to four different phases in the phase diagram.

(1) For $T > \max\big(T_{\mathrm{d}}(x), T_{\mathrm{sc}}(x)\big)$, the minimum is reached at $\alpha = 0$ and $\psi = 0$, which corresponds to the normal (N) phase. The section $T_{\mathrm{d}}(x)$ for $x < x_0$ is the line of phase transition from the N phase to the insulating OAF phase (α phase corresponding to a weak pseudogap), while the line $T_{\mathrm{sc}}(x)$ for $x > x_0$ corresponds to the phase transition from the N phase to the superconducting π phase.

(2) The insulating α phase penetrates the temperature range below $T_{\mathrm{sc}}(x)$ (the region of a strong pseudogap). The position of the $T_{\mathrm{C}}(x)$ line with $x < x_0$ corresponding to a phase transition from the α phase to the superconducting β phase is determined by the condition $b_2a_1 - b_{12}a_2 = 0$. In the α phase, $\psi = 0$ and $\alpha^2 = -a_2/b_2$.

(3) The sector β corresponds to the superconducting β phase in which

$$\psi^2 = -\frac{b_2a_1 - b_{12}a_2}{b_1b_2 - b_{12}^2} , \qquad \alpha^2 = -\frac{b_1a_2 - b_{12}a_1}{b_1b_2 - b_{12}^2} , \tag{13}$$

and superconductivity coexists with spontaneous orbital antiferromagnetism. The temperature T_{C} of superconducting phase transition from α to β phase is below T_{sc}. Similarly, the temperature $T_{\beta\pi}$ of the phase transition between two superconducting states (β and π phases) is less than T_{d}.

(4) In the superconducting π phase, the order parameter has the form $\alpha = 0$, $\psi = -a_1/b_1$. Part of the π phase between $T_{\mathrm{d}}(x)$ and $T_{\beta\pi}(x)$ for $x > x_0$ penetrates the temperature range below $T_{\mathrm{d}}(x)$.

Apart from the four thermodynamically distinct phases, the diagram shows two regions that can be interpreted as regions of developed fluctuations of the superconducting order parameter (the region between the $T_{\mathrm{sc}}(x)$ and $T_{\mathrm{C}}(x)$ lines for $x < x_0$) and the OAF order parameter (the region between the $T_{\mathrm{d}}(x)$ and $T_{\beta\pi}(x)$ lines for $x > x_0$). In the first of these regions it is the order parameter ψ that fluctuates: incoherent superconducting pairs exist in the form of quasistationary states at temperatures exceeding T_{C} [29]. The fluctuation state of superconducting pairs corresponds to the saddle point (on the ψ-axis) of the free-energy density as a function of ψ and α, close in energy to the minimum on the α-axis. The temperature T_{sc} up to which developed fluctuations of SC pairs exist is not the phase transition temperature and corresponds to the crossover between the two states of the insulating α phase: weak and strong pseudogaps. It should be noted that quasistationary states can also occur at temperatures above T_{sc} [29], thus extending the region relevant to the strong pseudogap.

In the region of developed fluctuations of the insulating order parameter α [between the lines $T_{\mathrm{d}}(x)$ and $T_{\beta\pi}(x)$ inside the superconducting state], the free-energy density passes a minimum on the ψ-axis and the saddle point on the α-axis. The free-energy values in the minimum and at the saddle point are close to each other within this region and the line $T_{\mathrm{d}}(x)$ has the meaning of crossover which limits conditionally the π-phase region with developed fluctuations of the insulating OAF order parameter α. These fluctuations appear as quasistationary states of orbital circular currents and correspond to the current circulations in the superconducting state, which were investigated in Ref. [30]. Such fluctuations occurring in the mean-field scheme are due to the competition between two ordered states. The second-order phase transition between two superconducting states at $T_{\beta\pi}(x)$ separates the region of conventional superconductivity (π phase), which is in fact described by the one-component order parameter (ψ), from the coexistence region of the insulating state and the SC state (β phase), whose description essentially requires no less than a two-component order parameter. Above the doping level corresponding to the $\beta \to \pi$ transition, a broad region of phase diagram exists which also shows up developed fluctuations. Since such a transition proceeds between two superconducting states, the phase interruption is due not to the motion of the center of mass but to the relative pair motion, i.e., to fluctuations of the relative phase β in the form of quasistationary states of circular orbital currents. Phase interruption of the superconducting order parameter (this phase is due to the motion of the center of mass of the pair) leading to the destruction of superconductivity results from the occurrence of Abrikosov vortices, which is the cause of the anomalous strengthening of the Nernst effect.

Our analysis is, strictly speaking, valid in only a small neighborhood of the tetracritical point c, and so the lines extended beyond this neighborhood have a rather conditional meaning reflecting the general tendencies of their behavior in the neighborhood of point c. In this connection, it should be noted that the extension of the line $T_{\beta\pi}(x)$ to the $T = 0$-axis up to $x = x_b$ (the line of second-order phase transition cannot end at a point) naturally leads to the concept of a quantum critical point ($x = x_b$, $T = 0$) for a higher doping level x_b compared to x_0.

In the case of a short-range rather than a long-range OAF order, the phase transition inside the superconducting state does not occur, and yet the broad region of developed fluctuations at temperatures above T_c allows interpretation of the pseudogap state with conditional separation into strong and weak pseudogaps, reflecting one of the admissible versions of the phase diagram of cuprates [42].

The conception of large-momentum superconducting pairing in screened Coulomb repulsion [20], which naturally leads to a two-component order parameter reflecting the charge and current degrees of freedom of the relative pair motion, agrees well on the whole with experimental data for the phase diagram and the physical properties of cuprates.

The work was supported by the Russian Foundation for Basic Research (grants Nos 05-02-17077a and 06-02-17186a).

References

1. Ginzburg V L, Landau L D *Zh. Eksp. Teor. Fiz.* **20** 1064 (1950) [Translated into English: *Collected Papers of L.D. Landau* (Oxford: Pergamon Press, 1965) p. 546]
2. Bardeen J, Cooper L N, Schrieffer J R *Phys. Rev.* **108** 1175 (1957)
3. Abrikosov A A *Zh. Eksp. Teor. Fiz.* **32** 1442 (1957) [*Sov. Phys. JETP* **5** 1174 (1957)]
4. Gor'kov L P *Zh. Eksp. Teor. Fiz.* **36** 1918 (1959) [*Sov. Phys. JETP* **9** 1364 (1959)]
5. Bednorz J G, Müller K A *Z. Phys. B* **64** 189 (1986)
6. Ginzburg V L, Kirzhnits D A (Eds) *Problema Vysokotemperaturnoi Sverkhprovodimosti* (The Problem of High-Temperature Superconductivity) (Moscow: Nauka, 1977) [Translated into English: *High-Temperature Superconductivity* (New York: Consultants Bureau, 1982)]
7. Bulaevskiĭ L N, Ginzburg V L, Sobyanin A A *Zh. Eksp. Teor. Fiz.* **94** 355 (1988) [*Sov. Phys. JETP* **67** 1499 (1988)]; Bulaevskiĭ L N, Ginzburg V L, Sobyanin A A, Stratonnikov A A *Usp. Fiz. Nauk* **157** 539 (1989) [*Sov. Phys. Usp.* **32** 277 (1989)]
8. Ginzburg V L *Zh. Eksp. Teor. Fiz.* **14** 177 (1944); *J. Phys. USSR* **8** 148 (1944); *Pis'ma Zh. Eksp. Teor. Fiz.* **49** 50 (1989) [*JETP Lett.* **49** 58 (1989)]; *Usp. Fiz. Nauk* **168** 363 (1998) [*Phys. Usp.* **41** 307 (1998)]
9. Ginzburg V L et al. *Solid State Commun.* **50** 339 (1984)
10. Corson J et al. *Nature* **398** 221 (1999)
11. Xu Z A et al. *Nature* **406** 486 (2000)
12. Wang Y et al. *Science* **299** 86 (2003)
13. Wang Y et al. *Phys. Rev. Lett.* **95** 247002 (2005); cond-mat/0503190
14. Anderson P W *Science* **235** 1196 (1987)
15. Dagotto E *Rev. Mod. Phys.* **66** 763 (1994)
16. Kohn W, Luttinger J M *Phys. Rev. Lett.* **15** 524 (1965)
17. Moskalenko V A *Fiz. Met. Metalloved.* **8** 503 (1959)
18. Suhl H, Matthias B T, Walker L R *Phys. Rev. Lett.* **3** 552 (1959)
19. Damascelli A, Hussain Z, Shen Z-X *Rev. Mod. Phys.* **75** 473 (2003)
20. Belyavsky V I, Kopaev Yu V *Usp. Fiz. Nauk* **176** 457 (2006) [*Phys. Usp.* **49** 441 (2006)]
21. Basov D N, Timusk T *Rev. Mod. Phys.* **77** 721 (2005)
22. Loram J W et al. *Physica C* **341–348** 831 (2000)
23. Belyavsky V I, Kapaev V V, Kopaev Yu V *Pis'ma Zh. Eksp. Teor. Fiz.* **81** 650 (2005) [*JETP Lett.* **81** 527 (2005)]
24. Sadovskiĭ M V *Usp. Fiz. Nauk* **171** 539 (2001) [*Phys. Usp.* **44** 515 (2001)]
25. Emery V J, Kivelson S A *Nature* **374** 434 (1995)
26. Chakravarthy S et al. *Phys. Rev. B* **63** 094503 (2001)
27. Lee P A, Nagaosa N, Wen X-G *Rev. Mod. Phys.* **78** 17 (2006)
28. Boebinger G S et al. *Phys. Rev. Lett.* **77** 5417 (1996)
29. Belyavskii V I et al. *Zh. Eksp. Teor. Fiz.* **126** 672 (2004) [*JETP* **99** 585 (2004)]
30. Ivanov D A, Lee P A, Wen X-G *Phys. Rev. Lett.* **84** 3958 (2000)
31. Belyavsky V I, Kopaev Yu V, Smirnov M Yu *Zh. Eksp. Teor. Fiz.* **128** 525 (2005) [*JETP* **101** 452 (2005)]
32. Belyavsky V I, Kopaev Yu V, Smirnov M Yu *Phys. Rev. B* **72** 132501 (2005)
33. Belyavsky V I et al. *Zh. Eksp. Teor. Fiz.* **124** 1149 (2003) [*JETP* **97** 1032 (2003)]
34. Belyavsky V I, Kopaev Yu V *Phys. Rev. B* **67** 024513 (2003)
35. Belyavsky V I et al. *Phys. Lett. A* **342** 267 (2005)
36. Franck J P, Lawrie D D *J. Supercond.* **8** 591 (1995)
37. Berk N F, Schrieffer J R *Phys. Rev. Lett.* **17** 433 (1966)
38. Chubukov A V, Pines D, Schmalian J, in *The Physics of Superconductors* Vol. 1 *Conventional and High-T_c Superconductors* (Eds K H Bennemann, J B Ketterson) (Berlin: Springer-Verlag, 2003) p. 495
39. Zhao G *Phys. Rev. B* **64** 024503 (2001)
40. Brandow B H *Phys. Rev. B* **65** 054503 (2002)
41. Belyavsky V I, Kopaev Yu V *Zh. Eksp. Teor. Fiz.* **127** 45 (2005) [*JETP* **100** 39 (2005)]
42. Norman M R, Pines D, Kallin C *Adv. Phys.* **54** 715 (2005); cond-mat/0507031

PACS numbers: **41.60.–m**, **52.20.–j**, 52.27.Lw
10.1070/PU2007v050n05ABEH006215

Polarization effects in a medium: from Vavilov–Cherenkov radiation and transition radiation to dust-particle pairing, or the development of one of V L Ginzburg's ideas from 1940 to 2006

V N Tsytovich

1. Polarization around particles

In the future general particle theory, with each particle consisting of all the other particles, any particle, being an excitation of the system, will be surrounded by the polarization of these other particles. So far, only the notion of the polarization produced around particles traveling through a medium has been elaborated (Fig. 1a). When the states of the particles change, their polarization 'coats' also change. Figure 1 shows the interaction of particles with external forces, with emitted radiation or incident radiation, with either individual incident particles or a large number of incident particles (i.e., particle fluxes) — the oval S in Fig. 1b. The interparticle interaction depends strongly on perturbations of the polarization cloud during the interaction. The physics of such interactions was first considered by Ginzburg [1].

2. Ginzburg's paper of 1940

In Ginzburg's 1940 paper "Quantum theory of the supersonic radiation of an electron uniformly traveling through a medium", quantum energy and momentum conservation laws for radiation in a medium, $\varepsilon_{\mathbf{p}} = \varepsilon_{\mathbf{p}'} + \hbar\omega_{\mathbf{k}}$ and $\mathbf{p} = \mathbf{p}' + \hbar\mathbf{k}$, were first used; in the system of units where $\hbar = 1$, they become $\varepsilon_{\mathbf{p}} = \varepsilon_{\mathbf{p}'} + \omega_{\mathbf{k}}$ and $\mathbf{p} = \mathbf{p}' + \mathbf{k}$, which in the classical limit ($\mathbf{k} \ll \mathbf{p}$, $\omega_{\mathbf{k}} \ll \varepsilon_{\mathbf{p}}$) leads to the classical Tamm–Frank condition $\omega_{\mathbf{k}} = (\mathbf{kv})$, $\mathbf{v} = \mathrm{d}\varepsilon_{\mathbf{p}}/\mathrm{d}\mathbf{k}$ for Vavilov–Cherenkov radiation. Of significance here is (i) the introduction of the photon momentum in the medium and (ii) the clear statement that an exchange of energy and momentum occurs only between the particle and the radiation. Subsequent research led to a deeper understanding and generalization of these statements.

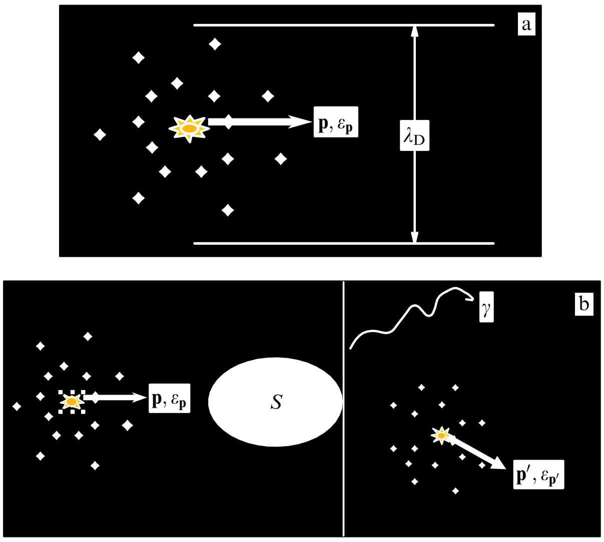

Figure 1. (a) A particle with a momentum **p** and energy $\varepsilon_{\mathbf{p}}$ freely moving through a medium is always surrounded by a polarization with some effective radius λ_{D} (the Debye radius in a plasma). (b) Scheme of the interaction of particles surrounded by polarization clouds: shown at the left is a particle prior to the interaction and at the right after the interaction, which results in the radiation of a mode of the medium (a wave propagating through the medium).

Concerning the first item, there is a remark in [1] that "...in a medium the photon momentum is $\hbar\omega n/c$ rather than $\hbar\omega/c$... the notion of photons with a momentum $\hbar\omega n/c$ is valid to the same degree as its related notion of the speed of light c/n, which is, strictly speaking, incorrect." Numerous subsequent investigations into the radiation in media with spatial dispersion confirmed this statement and enabled obtaining the general result that even in the classical description, the energy radiation power $\dot{E}$ and the momentum radiation rate $\dot{\mathbf{P}}$ obey the relations $\dot{E} = \int \omega_{\mathbf{k}} w_{\mathbf{k}}\, \mathrm{d}\mathbf{k}$ and $\dot{\mathbf{P}} = \int \mathbf{k} w_{\mathbf{k}}\, \mathrm{d}\mathbf{k}$, where $w_{\mathbf{k}}$ is the radiation probability. This result applies to any modes of the medium (for instance, phonons in solids or plasmons in a plasma) and even to those hydrodynamic modes whose electromagnetic momentum is zero or is negligible and is related to particle displacements. The second item turned out to be most important from the standpoint of physical consequences: any modes of the medium can be radiated by any heavy particles, the polarization of high-frequency waves being produced only by light particles (for instance, electrons) and therefore being determined by the mass of light particles. According to Ref. [1], only the particle and radiation can exchange momentum and energy, although polarization can be produced by light particles and determined by their mass (for instance, the radiation of an ion is determined by the electron mass).

This result appears to be more important than the widespread opinion that the most significant fact is that uniformly moving particles can emit radiation. This result also applies to other processes like transition (inherently polarization-related) scattering, polarization Bremsstrahlung, and the interaction of particles via their polarization clouds. All these lines of research have been under steady development, beginning with Ginzburg's paper [1], and are being pursued at present, including their numerous astrophysical applications. The most important of these areas are briefly discussed in the present report.

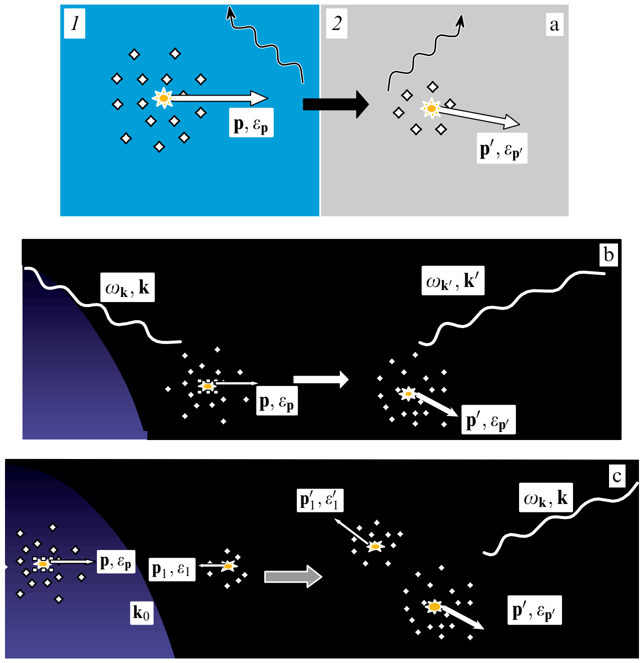

Figure 2. (a) During particle transit from medium *1* to medium *2*, modes (waves) in both media propagate from the interface and surface waves travel along the boundary between the media. The energy and momentum conservation law should account for a change in the particle polarization cloud in transit from medium *1* to medium *2*. (b) Transition scattering scheme: the incident wave gives rise to perturbations of the particle polarization cloud, which changes the scattering of heavy particles. (c) Scheme of particle polarization Bremsstrahlung, in which perturbations of all colliding-particle clouds during collisions play an essential role; the bound electrons of the polarization clouds of colliding atoms and ions also participate in the perturbations.

3. Patterns of transition radiation, transition scattering, and polarization Bremsstrahlung

Transition radiation, which was first considered by Ginzburg and I M Frank [2], is an example of a process related to polarization cloud variations in the transit of a particle from one medium to another, which leads to the radiation of modes in both media (Fig. 2a). The modes may be any modes of either media or surface modes. The energy and momentum conservation laws are satisfied only when the changes in the energy and momentum for the polarization 'fur coats' are taken into account, which is proven in Ref. [3]. Any mode or wave in the medium also carries a polarization wave with it; this polarization wave may be scattered due to the oscillations of the polarization cloud of the particle, which is transition radiation [4] (Fig. 2b). The transition radiation for ions in a plasma can be determined by the electron mass when the wavelength exceeds the polarization cloud size; therefore, the cross section for the scattering by ions can be greater than or of the order of the Thomson cross section for the scattering by electrons in the vacuum [5]. The transition scattering interferes with the ordinary scattering caused by the perturbation of motion of the scattering particle itself, and this interference suppresses the scattering by electrons.

The quantum scattering conservation laws $\varepsilon_{\mathbf{p}} + \omega_{\mathbf{k}} = \varepsilon_{\mathbf{p}'} + \omega_{\mathbf{k}'}$ and $\mathbf{p} + \mathbf{k} = \mathbf{p}' + \mathbf{k}'$, which are similar to those first used by Ginzburg for wave emission, lead to the law for the total scattering probability in the classical limit: $\omega_{\mathbf{k}} - \omega_{\mathbf{k}'} = (\mathbf{k} - \mathbf{k}')\,\mathbf{v}$. In particle collisions, the oscillation of the polarization cloud of each of the colliding particles makes a contribution to the amplitude of polarization–Bremsstrahlung radiation (Fig. 2c) [6]. The quantum conservation laws

$$\varepsilon_{\mathbf{p}} + \varepsilon_{\mathbf{p}_1} = \varepsilon_{\mathbf{p}'} + \varepsilon_{\mathbf{p}'_1} + \omega_{\mathbf{k}} ,$$
$$\mathbf{p}' = \mathbf{p} - \mathbf{k}_0 , \quad \mathbf{p}'_1 = \mathbf{p}_1 + \mathbf{k}_0 - \mathbf{k} ,$$

where $\mathbf{k}_0$ is the momentum transferred from one particle to another during collisions, lead to the same relation for the total emission probability in collisions in the classical limit as for the Bremsstrahlung with the perturbations of polarization clouds neglected: $\omega_{\mathbf{k}} = (\mathbf{k} - \mathbf{k}_0)\,\mathbf{v} + \mathbf{k}_0\mathbf{v}'$. The polarization clouds are like a 'transmission link,' but their perturbations may determine the energy and momentum exchange between the final states of radiation and particles [1].

4. Examples of transition scattering in plasmas

The measurement of the so-called Thomson scattering in plasma, which was carried out by British scientists invited to the USSR at the dawn of thermonuclear research, was used to prove the need for a sufficiently high temperature in tokamaks and lent impetus to the entire scope of research into controlled nuclear fusion. It is theorized that the scattering by individual particles is the Thomson scattering, i.e., occurs due to particle oscillations in the field of the incident wave, but in a plasma (or in another medium), this scattering corresponds to the scattering by density fluctuations and the resultant difference arises from the fact that electron density fluctuations may also be caused by ions.

The question arises as to the role of transition scattering in the total scattering. It is pertinent to note in this connection that, amazingly, some physicists are unaware of the foundations of the physical processes considered in Ref. [1] long ago. Physically, it is clear that for wavelengths longer than the polarization cloud size, the electrons of the cloud oscillate coherently in the wave field and the ions may scatter more intensely than the electrons, for which the polarization cloud oscillates in antiphase relative to the oscillations of the scattering electrons. The answer to this question, which was given in 1985 (published in the proceedings of the conference on transition radiation [7] held in Erevan), is as follows. When transition radiation is taken into account, the formulas used for the so-called 'Thomson scattering by fluctuations' can be rewritten as the sum of the scattering by electrons and ions. The scattering probability for electrons then contains the sum of the Thomson scattering and transition scattering amplitudes, while for ions the scattering is entirely determined by the transition scattering amplitude. This is also evident from the formula

$$\frac{Q}{Q_0} \propto r_0^2 \left[\left(1 - \frac{1-\epsilon_{\mathrm{e}}}{\epsilon} \right)^2 f_{\mathrm{e}} + \left(\frac{1-\epsilon_{\mathrm{e}}}{\epsilon} \right)^2 f_{\mathrm{i}} \right] ,$$

given in textbooks [8] on scattering in plasmas, where Q is the scattered radiation intensity, Q_0 is the incident radiation intensity, r_0 is the classical electron radius, ϵ_{e} and ϵ are the electron and total permittivities at the frequency and wave numbers of beats, and f_{e} and f_{i} are the electron and ion distribution functions. The difference between scattering by fluctuations and by separate particles is thereby eliminated: the total scattering is the sum of scatterings by separate particles. In the first approximation, this statement is valid for any medium. The transition scattering has resonances (zeroes of ε), which completely describe the experimentally measured Raman scattering from plasma modes. This treatment is not merely a different interpretation of scattering, because electrons and ions experience different types of additional actions (collisions at least).

The lack of understanding of transition scattering by astrophysicists is exemplified by the response of the editors of *Astrophysical Journal* to a paper submitted to that journal concerning the generalization of the Sunyaev–Zel'dovich effect to the low-frequency domain, where the transition scattering by ions with a cross section of the order of the Thomson scattering by electrons becomes dominant. The editors of one of the leading journals in astrophysics considered it possible to reply that "the authors may be right, but neither the Editors nor the referees can understand how ions can have such a large scattering cross section." The paper was published in the journal *Physics of Plasmas* [9]. This is indicative of the glacial pace with which physical notions laid back in 1940 [1] make their way to astrophysics.

5. Generalization of Einstein's notions of induced processes to nonequilibrium plasma states

Last year was the centenary of three Einstein's 1905 discoveries, including the discovery of stimulated processes, which provided the basis for modern laser physics. Plasma is the only medium where the smallness of field energy in comparison with the particle energy allows constructing an entirely analytic theory of nonequilibrium stimulated processes, including nonequilibrium distributions of plasma modes (determined by nonequilibrium numbers $N_{\mathbf{k}}$ of quanta) and plasma particles whose distribution is defined by nonequilibrium distributions f_{e} and f_{i}, with the inclusion of all stimulated processes [10]. The central results is the proof that this construction is possible only if polarization effects are taken into account in all processes. The probability of polarization scattering by ions appearing in Section 4 enters the nonequilibrium equation for the ion distribution function f_{i}. This leaves no room for doubt about the validity of the interpretation of scattering as a process whose inherent part is transition scattering; precisely the plasma ions gain energy and momentum in the course of such a scattering. Although the last statement may be derived using the results in Ref. [10], it was not explicitly formulated until 2005 (see report [11]). The experimental data published to date well indicate that ions are responsible for the stimulated transition scattering of plasma modes.

6. Examples of polarization Bremsstrahlung

Because the wavelength of a Bremsstrahlung photon is longer than the dimension of an atom, the role of a polarization cloud may also be played by bound electrons: for complex atoms, this effect was termed the atomic Bremsstrahlung or the polarization Bremsstrahlung radiation. The latter term reflects the fact that interference occurs, i.e., the amplitudes of the Bremsstrahlung and polarization radiation are added to each other.

Intensive theoretical investigations were performed and repeatedly borne out in experiments by a large team of the Leningrad Physicotechnical Institute and the teams of several Moscow institutes, including the Lebedev Physics Institute, the General Physics Institute, and the Kurchatov Institute. The main results are expounded in the collective monograph Ref. [6]. The following two examples serve to illustrate the possibility of manifestation of qualitatively new effects.

(1) In electron collisions with partially ionized atoms (ions) in a plasma, when the screening of an atomic nucleus is partly produced by bound electrons and partly by plasma electrons, the bound and free electrons may act coherently in the polarization Bremsstrahlung (the radiation intensity is proportional to the squared sum of the numbers of the bound and free electrons) [6, Ch. 6]. This occurs, of course, at a high speed of the incident particle, when its energy is much higher than the binding energy. In this case, the electrons bound prior to the collision remain such after the collision.

(2) In a plasma containing dust particles, the particles can lead to polarization Bremsstrahlung due to polarization charge oscillations in collisions of heavy dust particles. Dust particles carry very large negative charges (up to $Z_{\mathrm{d}} \approx 10^4 - 10^6$ in units of the electron charge), which are balanced by the cloud of the electrons and ions surrounding the dust particle. The Bremsstrahlung involves the standard smallness with respect to the coupling constant and the polarization radiation amplitude is of the same order of magnitude as the Bremsstrahlung amplitude, but the intensity, being proportional to the squared charge of each of colliding particles, contains a very large factor Z_{d}^4. In experiments, the polarization – Bremsstrahlung energy loss of dust particles due to the emission of low-frequency modes may be comparable to their energy loss due to deceleration in a neutral gas [12].

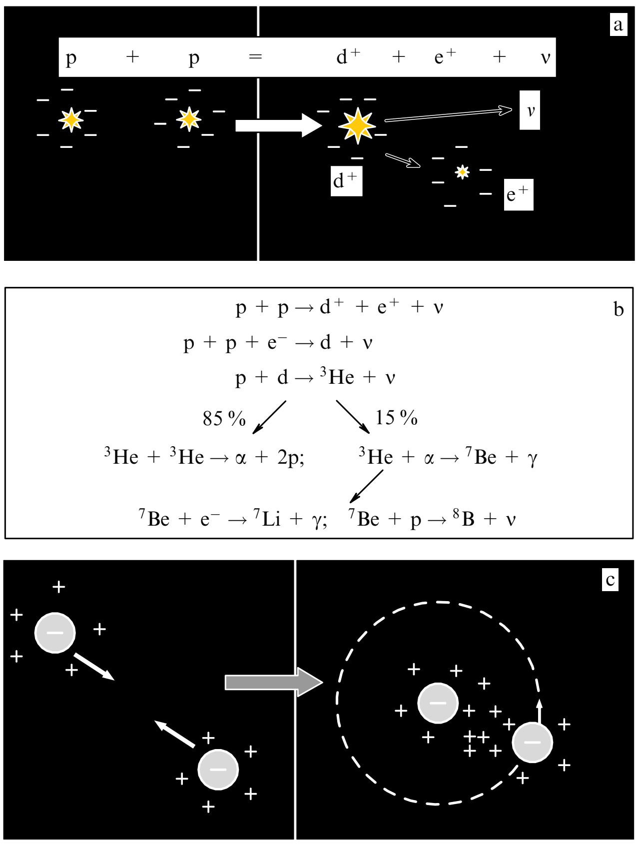

Figure 3. (a) Example of nuclear collisions at the beginning of the hydrogen cycle; prior to and after collisions, all charged particles of the nuclear reaction are surrounded by polarization clouds, which affect these reaction rates. (b) Scheme of the hydrogen cycle of nuclear reactions in the interior of the sun. Each of the nuclei is 'bare' (there are no bound electrons and the screening is effected by free negative charges of the plasma). (c) Formation of the bound states of two dust particles in their collisions, which is due to their attraction for an excessive density of positive ions of the polarization cloud between the interacting dust particles. The momentum and energy of a particle captured in an attractive potential well may decrease due to the emission of dust sound waves or friction against neutral gas atoms.

7. Particle collisions in a plasma

Nonradiative collisions that are also affected by the polarization clouds of particles are possible (Fig. 3a). It is generally accepted presently that particle interactions in collisions correspond to dynamically screened interactions, the polarization clouds in collisions of two selected (usually called probe) particles being formed by fluctuations of all the other plasma particles (see Ref. [5]). The two-particle collision cross sections contain the factor $1/|\epsilon_{\mathbf{k},\mathbf{k}\mathbf{v}}|^2$ and are therefore determined by the distributions of all the other plasma particles.

8. Effect of polarization on nuclear reaction rates

Normally, the polarization clouds affect nuclear tunneling, which is responsible for nuclear reactions (Fig. 3b). This is significant at high plasma densities of the order of the densities existing in the interior of stars, which was first pointed out by Salpeter [13] in 1954 and formed the basis for the modern scenario of stellar evolution. For the solar interior, corrections for the hydrogen cycle reactions (Fig. 3b) range from 5% to 20% [13]. The Debye screening was postulated in [13], although from the modern standpoint, such a screening must be derived in the fluctuation theory that takes nuclear reactions into account as well. The first such investigations [14] into the screening kinetics of nuclear reactions in a plasma exposed the main error in Ref. [13], which becomes evident when invoking the fluctuation theory that determines the final (and rather long) time of polarization screening formation.

Of significance in this problem is the understanding of the fundamental propositions that the description in quantum physics is probabilistic; specifically, the probabilistic nature of tunneling is an indication that although the tunneling time is short for a high barrier, its probability is low, which leads to low nuclear reaction rates. According to Ref. [14], the screening formation time due to fluctuations is much longer than the tunneling time. There also emerges a new effect: fluctuation correlations lead to an effect of the same order of magnitude as the increase in the tunneling probability due to the polarization lowering of the potential barrier. This effect was considered for the averaged Debye potential in Ref. [13]. As shown in Ref. [14], for a weak screening (roughly speaking, applicable to the solar interior), the amplitude of the correlation effect is precisely equal to the amplitude in Ref. [13]. But the sign of the correlation effect amplitude was calculated erroneously in Ref. [14], which would have been insignificant if both effects had been combined independently. However, the amplitudes, not the probabilities, are summed, and this led to destructive interference of the two effects in Ref. [14] (roughly speaking, if the Salpeter amplitude is taken to be 1, then $|1-1|^2 = 0$). With this error corrected in Ref. [15], the constructive interference of the two effects resulted in an unacceptable result: a four-fold increase in the corrections, $|1+1|^2 = 4$. A way out was also found in Ref. [15], where it was proven that the probabilities of the process do not change (with the fluctuation interpretation without the introduction of the unproven averaged screening) and the Salpeter effect is nonexistent. Then the correlations 'recover' the Salpeter result ($|1|^2 = 1$). But this is valid only for a weak screening, whereas the Salpeter effect is also used in the astrophysics of dense star evolution in conditions of strong screening. It has become necessary to replace it by strong correlation effects, whose theory is not yet fully elaborated, although there is a wide spectrum of laboratory experimental investigations [16].

9. Interaction and pairing of dust particles

In recent years, considerable experimental and theoretical study has been devoted to dust plasmas (see reviews [17, 18]). The central problem is the interaction of dust particles, which are macroscopic objects (with the number of atoms greater than $10^9 - 10^{11}$) with high negative charges (over $10^4 - 10^6$ electron charges) and with dimensions much shorter than the dimension of the polarization screening cloud. Each particle produces plasma flows and interacts with plasma flows, and polarization charges interact not with individual plasma particles but coherently with many of them or, to state it in different terms, with plasma flows. In the experiments conducted, the free path of the flows is indeed short and the flow field is the additional field whose interaction with the polarization field may change the interaction of dust particles (see the schematic in Fig. 3c). In this case, it turns out that repulsion becomes attraction at long distances, where the flows affect the particle interaction most efficiently (Fig. 4a), which signifies the possibility of particle pairing with the formation of bound states like dust molecules by like-charged particles and the possibility of forming larger dust particle complexes up to crystals. The experimental discovery of these crystals in 1996 [19 – 22], which were termed plasma crystals, posed the problem of explaining the physics of their formation. The change of the isolated dust particle interaction in plasmas due to plasma flows was first considered by Pitaevskii [23] in 1960, but the effect of the flows on the interaction of isolated particles is substantially different from that for a collection of dust particles.

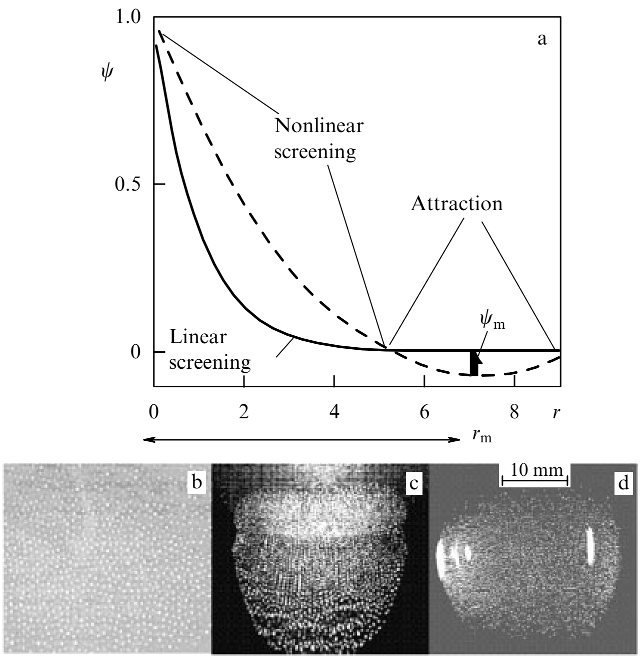

Figure 4. (a) Schematic representation of the screening factor ψ in the interaction of dust particles, $V = Z_d^2 e^2 \psi(r/\lambda_{Di})/r$; the interparticle distance r is given in terms of λ_{Di}. (b, c, d) Examples of the plasma crystals observed in Refs [19, 22, 33], respectively. Shown in Fig. 4b is the distribution in one of the crystal planes; in Figs 4c and 4d, the vertical axis is oriented along the force of gravity in the laboratory experiments in Refs [22, 33].

Indicated in Fig. 4a is the domain of collective interaction for two probe particles, which emerges in the presence of many-particle flows and is basically similar to collective interaction in ordinary plasmas (see Section 7). The collision integrals that describe the dust particle interactions contain not only the mean-square fluctuations of polarization fields but also the mean products of the polarization fields and the flow fields, which are related to each other. A significant feature of the interaction is the nonlinearity of the polarization cloud; this effect first considered in Ref. [24] for artificial earth satellites (their dimensions are also shorter than the screening radius), and is commonly called the Gurevich screening in the literature.

10. Plasma dust crystals and explanation of phase transition parameters

It was believed that the high charges of plasma dust particles could lead to strong correlations and could be responsible for the transition of dust to a crystal state even at low dust density [25]. It was assumed that the coupling constant (nonideality constant) $\Gamma = Z_d^2 e^2 / T_d r_m$ (where $r_m = (4\pi n_d/3)^{-1/3}$ is the average distance between the dust particles and T is the dust temperature) in this case should amount to at least $4 - 10$, as for ordinary phase transitions to the solid state. The ease of crystal production from dust in plasmas by the mere injection of dust particles into an ordinary high-frequency discharge in a low-temperature plasma [19] (it was even sufficient to inject printer toner [26]) and especially the transition parameters themselves [27, 28] turned out to be quite unexpected (examples of dust crystals obtained in different experiments are given in Figs 4b – 4d).

The first surprising thing is that the observed values of the parameter Γ are extremely large (from $\approx 3 \times 10^3 - 10^4$ up to $\approx 10^5$). Second, the value of r_m is relatively large and exceeds the linear screening radius by a factor of $8 - 10$. If the dust particle field is assumed to be completely screened at these distances, it is unclear why the particles do not come closer to each other. Lastly, the dust temperature T_d on crystal melting turned out to be rather low, of the order of $0.1 - 1$ eV. Although this temperature is much higher than room temperature (≈ 0.02 eV) and the crystals are rather 'firm,' it is much lower than the maximum energy that corresponds to the approach of particles for a distance of the order of their radius, which is estimated as $3 Z_d T_e \approx 50$ keV for the values $Z_d \approx 3 \times 10^3$ and $T_e \approx 2$ eV, typical for the experiments conducted.

This brings up the question: Is it mere coincidence that the large observed magnitude of Γ agrees with the ratio between the maximum interaction energy and the melting temperature? The crystal formation can hardly be called a manifestation of strong coupling, because the interaction might be many times stronger. The interaction is most likely the unscreened Coulomb interaction, which is confirmed by abundant experimental evidence for the attraction of like-charged dust particles [29, 30]. Initially, attempts were made to fit the observed Γ values to the value $\Gamma = 170$ predicted numerically for a one-component plasma model by invoking the Debye screening. However, the value of the screening length should then be restricted by certain bounds: the screening radius may differ from the interparticle distance no greater than several-fold, which gives an unacceptably long screening radius. Furthermore, it became evident that such screening, unlike the linear Debye screening, is nonlinear, because the ratio between the potential energy and the temperature of screening ions ranges from ≈ 300 to $3-10$ in a broad domain around the dust particle. The best explanation was obtained with the inclusion of the interaction of flux fields and polarization fields for nonlinear screening [31, 32] responsible for dust particle attraction, which is schematically shown in Fig. 4a. This model not only predicts the correct value of the interparticle distance but also easily explains other observations: the large value of $\Gamma = 1/\psi_m$ [31, 33] and the low ratio between the melting temperature and the maximum interaction energy, which turns out to be equal to ψ_m, this ratio coinciding with $1/\Gamma$. The screening nonlinearity is significant in this case because it determines the polarization charge distribution in the nonlinear domain near the dust particle and defines the interparticle distance at which an energy minimum of the attractive well occurs, close to the observed interparticle distance r_m.

The attraction of dust particles exists irrespective of whether the screening is linear or nonlinear, the nonlinearity normally being strong in laboratory experiments, where $\tau = T_i/T_e \approx 10^{-2}$, and most often weak under astrophysical conditions. In all cases, the particle fields are modified by the flows such that they become long-range and extend to distances much longer than the Debye screening radius. There has been significant progress in solving this problem, but it is still unclear how to introduce, even if approximately, free energy in a manifestly non-Hamiltonian system in order to gain the possibility of using standard models of phase transitions. It is pertinent to note that this research shows promise for studying the effects of pairing (of electrons, in particular) in other nonequilibrium systems.

11. Effective gravitational instability in a dust plasma

The long-range attraction of dust particles and the fact that a certain part of their field is not completely screened and extends to long distances may lead to a new, gravitational-type instability in dust plasmas [34, 35]. Only dust particles are subject to this instability, while the ordinary universal gravitational instability acts on any mass. Of course, attraction may also be transferred to other particles via the interaction with the dust particles. In laboratory conditions, this instability may lead to the formation of different structures that may experience a phase transition to the crystal state on further cooling of the dust particles. In astrophysical conditions, it may be associated with the observed structuring of dust clouds with dimensions much shorter than the Jeans length for the ordinary gravitational instability.

The dispersion equation for the effective dust instability coincides in form with the well-known equation for the ordinary gravitational instability $\omega^2 = k^2 v_{s,\,\mathrm{eff}}^2 - G_{\mathrm{eff}}\, m_d n_d$, which is written, for example, for dust particles with a specific mass m_d, size a, and density n_d. The effective speed of sound corresponds to the dust sound speed [35],

$$v_{s,\,\mathrm{eff}}^2 = \frac{Z_d P T_i}{m_d s_{\mathrm{eff}}}\,, \quad s_{\mathrm{eff}} = \frac{1+P}{1+z}\,,$$

where $P = n_d Z_d / n_i$ is the parameter characterizing the relative charge fraction on dust particles (normally, of the order of unity) and $z = Z_d e^2 / a T_e$ is the dimensionless charge of the dust particles (equal to about $2-4$). The effective gravitational constant G_{eff} depends on the coupling constant $k_{\mathrm{eff}}\lambda_D$ of flows to electromagnetic fields ($1/k_{\mathrm{eff}}$ is of the order of the most effective length of the interaction of electrostatic fields and flows) [32]:

$$G_{\mathrm{eff}} = \frac{Z_d^2 e^2 (k_{\mathrm{eff}}\lambda_D)^2}{m_d^2 s_{\mathrm{eff}}}\,(k_{\mathrm{eff}}\lambda_D)^2 = \frac{\alpha_d z a^2 T_e}{T_i \lambda_{Di}^2}\,,$$

where α_d is a numerical constant, which is estimated as $\alpha_d \approx 0.16$ and depends on the coefficients determining the charging rate of dust particles and the force of their entrainment by ion flows. The effective Jeans length $L_{\mathrm{eff}} \approx 1/k_{\mathrm{eff}}$, independent of the mass of dust particles and only slightly dependent on their size, may be estimated using the number of ions inside the sphere of the ion Debye radius $N_i = n_i 4\pi\lambda_{Di}^3/3$ as

$$L_{\mathrm{eff}} \approx \lambda_{Di}\,\frac{N_i}{Z_d}\,\sqrt{\frac{T_e(1+z)}{T_i\,\alpha_d P\,(1-P)}}\,.$$

For typical parameters of laboratory experiments, $a \approx 10\ \mu$m, $z \approx 3$, $T_e \approx 3$ eV, $m_d \approx 2\times10^{-9}$ g, and $P \approx 0.5$, we obtain $G_{\mathrm{eff}} \approx 72.6$ dyn cm^2 g^{-2}, i.e., G_{eff} is approximately nine orders of magnitude greater than the ordinary gravitational constant $G = 6.67\times10^{-8}$ dyn cm^2 g^{-2}. The effective Jeans length and the effective dust particle attraction correspond to those appearing in the explanation for dust crystallization in laboratory experiments. In astrophysical conditions, the effective Jeans length is estimated differently for dust clouds of various types but is normally in the $10^{14}-10^{17}$ cm range and, as a rule, turns out to be much shorter than the gravitational Jeans length.

Polarization effects also have numerous astrophysical applications.

12. Transition scattering in the interior of the sun and solar neutrinos

Thermonuclear reactions in the interior of the Sun [in its central part, up to approximately $(1/3)R_\odot$] heat the interior to $T \approx 1.5$ keV, and the energy transfer to the solar surface is radiatively effected due to scattering by electrons and ions. The scattering by ions is transition scattering and practically replaces the scattering by electrons in the frequency range $\omega_{pe} < \omega \ll \omega_{pe} c/v_{T_e}$, where ω_{pe} is the electron plasma frequency, c is the speed of light, and v_{T_e} is the average thermal electron velocity. The solar opacity is determined by scattering processes, and this coefficient is used in solar models to determine the interior temperature from the observed luminosity and thereby to determine the neutrino flux. Depending on the temperature, most critical is the yield of highest-energy neutrinos in the hydrogen cycle (the boron neutrinos from the decay of ^{7}Be, producing ^{8}B, in particular), which were measured in David's first experiments with a deficit of $2-3$.

A very strong temperature dependence of the boron neutrino yield corresponds to the fact that a temperature decrease by $1-2$ K in the solar interior results in a reduction in the number of energetic neutrinos by about a factor of 2. The $1-2$ K temperature decrease does not contradict solar seismology data, although the accuracy of solar vibration mode measurements decreases sharply for the modes that extend to the central solar region. That is why the role of ions in the scattering and transfer of radiation in the solar interior did not attract attention until 1987 in connection with the problem of solar neutrino deficit [36]. In Ref. [36], the problem was considered in the framework of scattering by electron fluctuations under the assumption that ions affect these fluctuations. As already discussed in detail, this essentially amounts to describing the transition scattering by ions in the first approximation; in this approximation, the results in Ref. [36] are correct and take the transition scattering by ions into account. The criterion that the scattering by ions is dominant is not quite well satisfied in the solar interior, and therefore about 30–60% of the radiation energy is scattered by ions and accordingly 40–70% by electrons, depending on the radiation frequency. This is because the frequency range for the propagation of electromagnetic waves in the solar interior is rather narrow: $\omega_{\rm pe} \approx 9.78 \times 10^{17} < \omega < T/\hbar \approx 7.62 \times 10^{18}\ {\rm s}^{-1}$, while $c/v_{T_{\rm e}} \approx 10.1$, and therefore the condition $\omega \ll \omega_{\rm pe}(c/v_{T_{\rm e}})$ for strong dominance of the scattering by ions is not satisfied, strictly speaking. In the calculations in Ref. [36], the effects of transition scattering by ions in the models of radiation transfer in the solar interior are included only in the first approximation. Further improvements in opacity (after the required revision of the interpretation) called for a clear differentiation between the effects affecting the radiation transfer by ions and those affecting the radiation transfer by electrons. An investigation into additional corrections to the opacity coefficient (there are nine of them in all), which was generalized in Ref. [37], shows that the total of all corrections may amount to 7–12%, which yields an interior temperature decrease by 1–2 K, which is required by high-energy solar neutrinos, for practically invariable proton neutrino fluxes.

13. Polarization corrections to thermonuclear reactions and solar neutrinos

A polarization effect in the solar interior that affects the neutrino yield is the correlation of fluctuations producing the polarization clouds, which, as discussed above, coincide with the Salpeter factor [13] only in the first order. A more detailed analysis of the correlation effects in polarizations and their role in all reactions of the hydrogen cycle (Fig. 3b) was performed in Ref. [15]. It revealed that the corrections to almost all of these reactions are 1.25–1.37 times greater than the Salpeter corrections. The latter increase from 5% early in the hydrogen cycle to 20% at the end of the cycle. According to Ref. [15], only correlation effects can be responsible for corrections to the thermonuclear reaction rates, and therefore the corrections increase from 6.5% to 25%. This does not have a marked effect on the predictions for the neutrino radiation from the first reactions of the hydrogen cycle and is in reasonable agreement with observations.

But the correlation corrections for reactions with ^{7}Be at the end of the hydrogen cycle are of the opposite sign (suppression rather than enhancement of the reactions) and are three times greater in absolute value than the Salpeter corrections. This is yet another effect that may account for the observed energetic neutrino deficit in David's experiments, irrespective of whether neutrino oscillations exist.

We note that there persist theoretical problems associated with low-energy neutrinos early in the hydrogen cycle. The correlation corrections coincide with the Salpeter ones only in the first order under the assumption of weak screening. However, earlier in the construction of solar models, it was noted that the screening is not very weak and the parameter characterizing its smallness is not much smaller than unity (is equal to about 1/7), and formulas interpolating between weak and strong Salpeter screening were used in constructing solar models. According to Ref. [15], the Salpeter screening is replaced by correlation effects whose theory may be adequately elaborated only for weak correlations. There is no well-established theoretical result for strong correlations that might be used for interpolating the weak-screening result.

14. Stellar evolution

The problem related to correlation effects and to strong screening is aggravated for stars in which the hydrogen cycle was completed and whose combustion is associated with the carbon cycle. The nucleus of carbon ^{12}C has $Z = 6$, and the screening parameter is close to unity or much greater than unity. Weak screening may not be used, and there is still no good theory of strong screening related to strong correlations. The stellar evolution theory therefore invites a certain revision.

15. Sunyaev–Zel'dovich effect and transition scattering

The Sunyaev–Zel'dovich effect corresponds to photon reddening due to the induced scattering in radiation transit through a plasma. At present, only the Thomson scattering by electrons is taken into account and the effect is used for detecting the electron density. At frequencies $\omega < \omega_{\rm pe} c/v_{T_{\rm e}}$, transition scattering by ions is significant, while for $\omega \ll \omega_{\rm pe} c/v_{T_{\rm e}}$ transition scattering by ions prevails and the Sunyaev–Zel'dovich effect changes [9]. The wavelength threshold can be written in the form $\lambda > 47$ [m] $\sqrt{T\,[\mathrm{eV}]/n\,[\mathrm{cm}^{-3}]}$ and is manifested in the meter wavelength range for low temperatures and high densities of the plasma.

16. Transition scattering from dust particles forming noctilucent clouds

Noctilucent clouds are observed in the lower ionosphere at the altitude about 90 km in northern latitudes in summer. Radar detection by backscattering has revealed an abnormally high intensity of the scattered signal in comparison with the ordinary signal intensity due to scattering by electrons (approximately two orders of magnitude higher [38]). The simplest explanation is that the scattering is related to the transition scattering involving the nonlinear electron cloud of dust particles, which is consistent with the observation of a very small Doppler shift of the signal frequency indicating a very low scatterer speed. The scattering is proportional to $Z_{\rm d}^2 n_{\rm d} = Z_{\rm d} P n_{\rm i}$, and for the ordinary values $n_{\rm i} \sim n_{\rm e}$, $P \sim 1$, and $Z_{\rm d} \sim 100$ yields an increase in the scattered signal in qualitative agreement with observations [38].

17. New dust structures. Dust stars

The attraction of dust particles via polarization 'fur coats' may have several astrophysical consequences presently amenable to measurements. The observation of diversified dust structures in laboratory conditions led to the assumption that structuring processes are an inherent property of dust plasmas and may be attributed to the effective gravitational instability of dust systems. There are no grounds to believe that such processes cannot develop under astrophysical conditions in dust clouds. The main implication of the ordinary gravitational instability is the structuring of matter in space, and it is easily seen that the effective gravitational instability in dust plasmas should lead to the structuring of dust clouds. The structural property of such clouds is indeed observed, but it has not been analyzed to what extent it is attributable to the effective gravitational instability of dust plasmas. A prerequisite for this analysis is the progress in describing systems with a size spread of dust particles, but investigations in this area are still in their infancy.

However, one may set up the problem of the final stage of the process, as well as raise the following question: If the ordinary gravitational instability can lead to star formation, can the effective gravitational dust instability lead to the formation of 'dust stars' as isolated objects surrounded by dust-free domains? So far, the existence of stable equilibrium in spherical dust structures has been proven to be possible for all its components — dust, plasma particles, and dust particle charge [38]. The generalization to systems with a size distribution of dust particles and their consequential charge distribution has not been made so far. However, some qualitative implications of investigations performed up to now allow the following preliminary conclusions:

(i) all dust structures should have sharp boundaries;

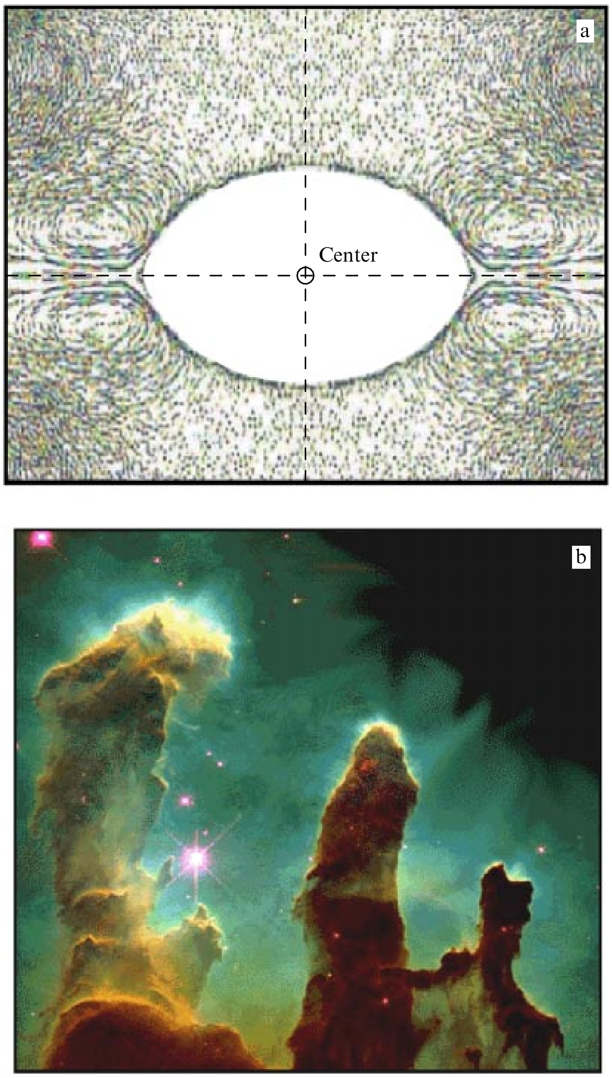

Figure 5. (a) Dust structures observed on the International Space Station. The central dust void, which is produced by plasma flows generated by ionization processes, has very sharp boundaries. On the outside, the dust plasma is surrounded by boundary voids, and convective dust cells are observed at the void periphery. Large-size dust structures break up into dust blobs (dust structures) and dust voids. (b) Example of dust structures with sharp boundaries in a dust nebula observed with the Hubble telescope.

(ii) dust stars should 'feed on' external plasma streams (i.e., should absorb plasma unlike ordinary stars, being 'antistars' in this respect);

(iii) convective flows caused by the nonpotentiality of the electrostatic forces acting on the dust particles due to the spatial inhomogeneity of their charge should develop in the boundary regions.

Both effects — the sharp boundaries of the dust structures and the formation of dust convection in them — are borne out by experiments onboard the International Space Station (Fig. 5a) [40], while the sharp boundaries of space dust clouds are clearly illustrated by one of the pictures made by the Hubble telescope (Fig. 5b). It is believed that many dust structures (in particular, of the 'dust star' type) might be discovered near the closest stars with the use of the instrumentation of the recently launched Spitzer infrared telescope.

Today, it is quite difficult to answer the question of the possible evolution of 'dust stars' and their possible contribution to hidden mass.

Planar dust structures like planetary rings may exhibit structuring when the gravity of the central planet is weaker than the effects of mutual dust particle attraction. This does not apply to those rings in which large particles (stones) are the main components, whose motion is controlled primarily by the gravity of the central planet. A typical polarization effect like the excitation of the Mach cones of dust sound by a big stone [41] flying under one of Saturn's rings has now been planned for experiments using the Cassini space instrument, which has been successfully orbiting in the Cassini division for more than a year. The attraction of dust particles may show up in the Vavilov – Cherenkov radiation of the dust sound only when the spectrum is measured to sufficiently long wavelengths, of the order of those for which the effective gravitational instability discussed above may be significant.

The aim of this report was to show that the simple and yet extremely keen observations made by Ginzburg in 1940 have far-reaching implications and open up new vistas for laboratory and astrophysical investigations, including investigations into the pairing mechanisms of like-charged particles in nonequilibrium systems.

References

1. Ginzburg V L *Zh. Eksp. Teor. Fiz.* **10** 589 (1940); *J. Phys. USSR* **2** 441 (1940)
2. Ginzburg V L, Frank I M *Zh. Eksp. Teor. Fiz.* **16** 15 (1946); *J. Phys. USSR* **9** 353 (1945) (brief version)
3. Ginzburg V L, Tsytovich V N *Perekhodnoe Izluchenie i Perekhodnoe Rasseyanie* (Transition Radiation and Transition Scattering) (Moscow: Nauka, 1984) [Translated into English (Bristol: A. Hilger, 1990)]
4. Ginzburg V L, Tsytovich V N *Zh. Eksp. Teor. Fiz.* **65** 1818 (1973) [*Sov. Phys. JETP* **38** 909 (1974)]
5. Tsytovich V N *Lectures on Non-Linear Plasma Kinetics* (Berlin: Springer, 1995)
6. Tsytovich V N, Oiringel' I M (Eds) *Polyarizatsionnoe Tormoznoe Izluchenie Chastits i Atomov* (Polarization Bremsstrahlung of Particles and Atoms) (Moscow: Nauka, 1987) [Translated into English (New York: Plenum Press, 1992)]
7. Ginzburg V L, Tsytovich V N, in *Materialy Mezhdunarodnoi Konf. po Perekhodnomu Izlucheniyu* (Proc. of the Intern. Conf. on Transient Radiation) (Erevan: EGU, 1985) p. 511
8. Sheffield J *Plasma Scattering of Electromagnetic Radiation* (New York: Academic Press, 1975) [Translated into Russian (Moscow: Atomizdat, 1978) p. 119]

9. Bingham R, Tsytovich V N, de Angelis U, Forlani A, Mendonça J T *Phys. Plasmas* **10** 3297 (2003)
10. Tsytovich V N *Teoriya Turbulentnoi Plazmy* (Moscow: Atomizdat, 1971) [Translated into English: *Theory of Turbulent Plasma* (New York: Consultants Bureau, 1977)]
11. Tsytovich V, in *EPS 13 Beyond Einstein Physics for the 21st Century. 13 Gen. Conf. Eur. Phys. Soc., Bern, Switzerland 11 – 15 July 2005*; *Europhys. Conf. Abst.* **29D** 97 (2005)
12. Goree J, Morfill G, Tsytovich V N *Fiz. Plazmy* **24** 534 (1998) [*Plasma Phys. Rep.* **24** 490 (1998)]
13. Salpeter E E *Austral. J. Phys.* **7** 373 (1954)
14. Tsytovich V N, Bornatici M *Fiz. Plazmy* **26** 894 (2000) [*Plasma Phys. Rep.* **26** 840 (2000)]
15. Tsytovich V N *Zh. Eksp. Teor. Fiz.* **121** 1080 (2002) [*JETP* **94** 927 (2002)]
16. Fortov V, in *Invited Papers from the 30th European Physical Society Conf. on Controlled Fusion and Plasma Physics* (*St. Petersburg, Russia, 7 – 11 July 2003*); *Plasma Phys. Controll. Fusion* **45** (12A) A1 (2003)
17. Tsytovich V N, Morfill G E, Thomas H *Fiz. Plazmy* **28** 675 (2002) [*Plasma Phys. Rep.* **28** 623 (2002)]; Morfill G E, Tsytovich V N, Thomas H *Fiz. Plazmy* **29** 3 (2003) [*Plasma Phys. Rep.* **29** 1 (2003)]; Thomas H, Morfill G E, Tsytovich V N *Fiz. Plazmy* **29** 963 (2003) [*Plasma Phys. Rep.* **29** 895 (2003)]; Tsytovich V N, Morfill G E, Thomas H *Fiz. Plazmy* **30** 877 (2004) [*Plasma Phys. Rep.* **30** 816 (2004)]
18. Fortov V E et al. *Usp. Fiz. Nauk* **174** 495 (2004) [*Phys. Usp.* **47** 447 (2004)]; *Phys. Rep.* **421** 1 (2005)
19. Thomas H et al. *Phys. Rev. Lett.* **73** 652 (1994)
20. Chu J A, Lin I *Physica A* **205** 183 (1994)
21. Hayashi Y, Tachibana K *Jpn. J. Appl. Phys.* **33** L804 (1994)
22. Fortov V E et al. *Phys. Lett. A* **219** 89 (1996)
23. Pitaevskii L P *Zh. Eksp. Teor. Fiz.* **39** 1450 (1960) [*Sov. Phys. JETP* **12** 1008 (1961)]
24. Al'pert Ya L, Gurevich A V, Pitaevskii L P *Iskusstvennye Sputniki v Razrezhennoi Plazme* (Artificial Satellites in Tenuous Plasmas) (Moscow: Nauka, 1964) [Translated into English: *Space Physics with Artificial Satellites* (New York: Consultants Bureau, 1965)]
25. Ikezi H *Phys. Fluids* **29** 1764 (1986)
26. Tomme E B, Annaratone B M, Allen J E *Plasma Sources Sci. Technol.* **9** 87 (2000)
27. Tsytovich V N *Pis'ma Zh. Eksp. Teor. Fiz.* **81** 563 (2005) [*JETP Lett.* **81** 448 (2005)]
28. Tsytovich V *Contrib. Plasma Phys.* **45** 533 (2005)
29. Law D et al., in *XXIII Intern. Conf. on Phenomena in Ionized Gases; ICPIG, Contrib. Papers* Vol. 1 (1997) p. 192
30. Annaratone B M et al. *Phys. Rev. E* **63** 036406 (2001)
31. Tsytovich V N *Zh. Eksp. Teor. Fiz.* **131** 312 (2007) [*JETP* **104** 279 (2007)]
32. Tsytovich V, Morfill G, in *Invited Papers from the 31st European Physical Society Conf. on Plasma Physics, London, UK* (*28 June – 2 July 2004*); *Plasma Phys. Controll. Fusion.* **46** (12B) B527 (2004)
33. Konopka U et al. *Phys. Rev. E* **61** 1890 (2000)
34. Tsytovich V N, Watanabe K *Contrib. Plasma Phys.* **43** 51 (2003)
35. Tsytovich V N *Phys. Scripta* **74** C81 (2006)
36. Boercker D B *Astrophys. J. Lett.* **316** L95 (1987)
37. Tsytovich V N et al. *Usp. Fiz. Nauk* **166** 113 (1996) [*Phys. Usp.* **39** 103 (1996)]
38. Havnes O, Aslaksen T, Brattli A *Phys. Scripta* **T89** 133 (2001)
39. Tsytovich V N *Comments Phys. Pt. E Comments Plasma Phys. Controlled Fusion* **1** 1 (2000)
40. Tsytovich V N *Fiz. Plazmy* **31** 157 (2005) [*Plasma Phys. Rep.* **31** 133 (2005)]
41. Havnes O et al. *Planet. Space Sci.* **49** 223 (2001)